

Chapter 4

Results and Discussion

4.1 *Pre-fatigue test phase*

The characterization of surface treated specimens was done for parameters like coating thickness, hardness, composition and surface roughness. Details are given in following sections.

4.1.1 Measurement of thickness / depth of coating:

Surface treatments which do not involve diffusion of species are characterized for the thickness of surface layer (e. g. chrome plating and thermal spray coating), while the one involving diffusion were subjected to measurement of its depth of diffusion layer (i.e. case depth, e.g. plasma nitriding). Figure 4.1 to 4. 4 give the micrographs demonstrating measurement of thickness of the specimens subjected to different surface treatments. The results obtained in each case are given as average thickness in Table 4.1.

Table 4.1: Data on coating thickness / case depth for specimens of different surface treatments

Specimen Category	Average coating thickness / Case depth
Untreated (base material)	Not applicable
Hard chrome plated	55 to 60 μm
Thermal spray coated (alumina)	475 to 525 μm
Plasma nitrided- Total case depth	400 to 450 μm
Plasma nitrided- Compound layer (white layer) thickness	0 to 20 microns

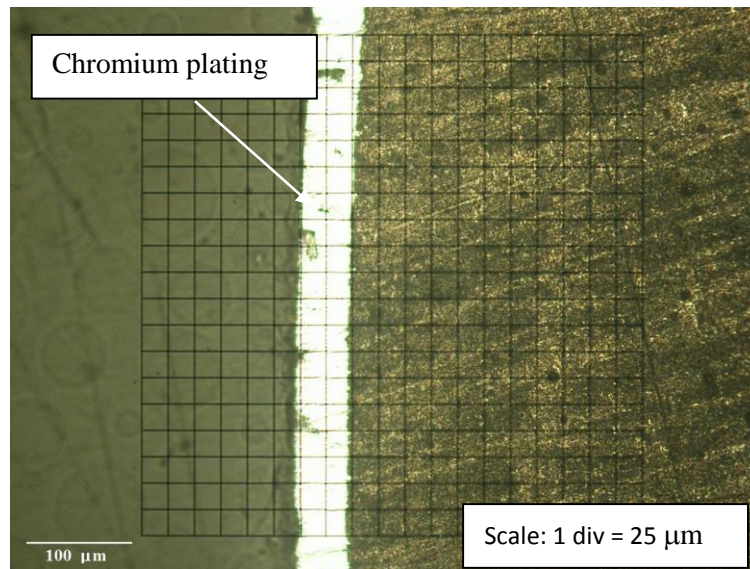


Fig. 4.1: Micrograph for hard chrome plated specimen subjected to thickness measurement.

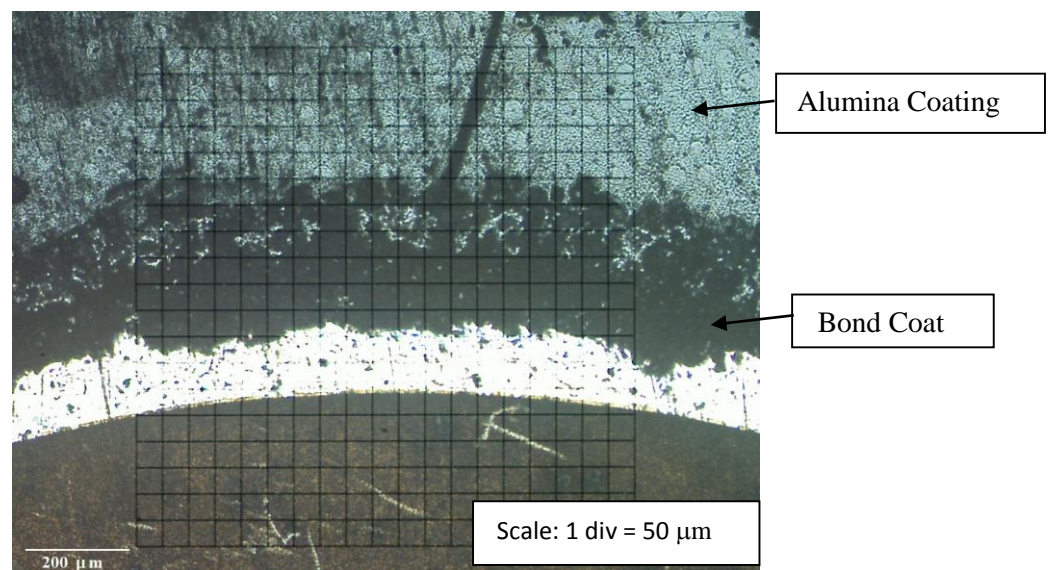


Fig. 4.2: Micrograph for thermally- sprayed with alumina specimen subjected to thickness measurement

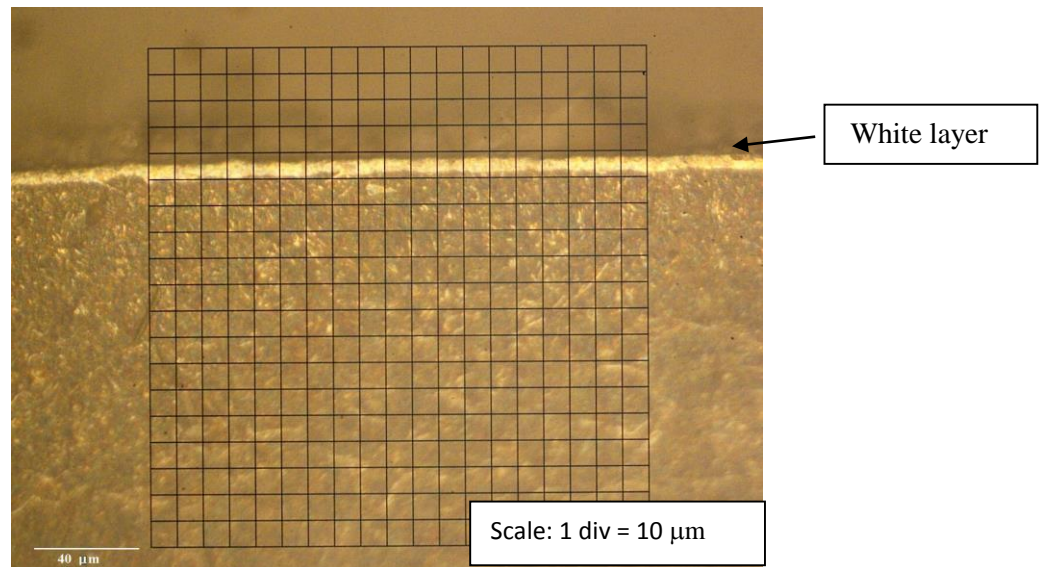


Fig. 4.3: Micrograph for plasma nitrided specimen subjected to thickness measurement having white layer of $< 10 \mu\text{m}$

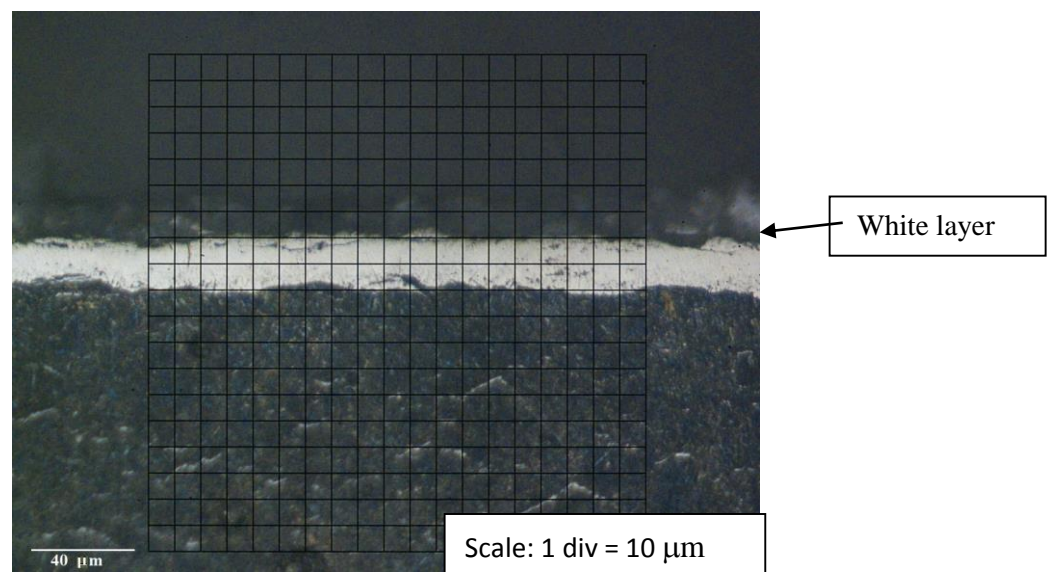


Fig. 4.4: Micrograph for plasma nitrided specimen subjected to thickness measurement having white layer of $> 10 \mu\text{m}$

4.1.2 Surface roughness measurements:

Table 4.2 gives the data on surface roughness (R_a value) for specimens of different surface treatments. The data indicate that except for thermal spray coating, all other surface treatments offer surface layers have better surface finish than base material. Lower the R_a value greater is the surface finish. Thus thermal spray coated specimens have highest surface roughness i.e. very poor surface finish. Surface finish of the material has an effect on its fatigue behaviour. For example, ground and polished

specimens offer better fatigue life than ground and un-polished specimens, as the probability of initiation of a fatigue crack from the surface is higher in the latter case.

Table 4.2: Data on surface roughness (R_a value) for specimens of different surface treatments

Category	Average surface roughness (R_a) in microns
Untreated (base material)	0.68
Hard chrome plated	0.35
Thermal spray coated (alumina)	7.49
Plasma nitrided	0.49

4.1.3 Measurement of surface hardness:

The surface hardness was measured using portable hardness tester based on ultrasound principle in case of specimens prepared by chrome plating as well as thermal sprayed coating, while it was measured using microhardness tester for plasma nitrided specimens. The microhardness measurements were made from surface towards core and the microhardness values were plotted against distance from the surface. The data on surface hardness for all categories of surface treatments are given in Table 4.3, while the data on microhardness as well as microhardness profile for plasma nitrided specimens are given in Table 4.4 and Fig. 4.5, respectively.

Table 4.3: Surface hardness for specimens of different surface treatments

Category	Hardness (average value)
Untreated / base material	32±2 HRc
Chrome plated	700 -750 Hv
Thermal spray coated (alumina)	1100 -1200 Hv
Plasma nitrided	700-750 Hv

Table 4.4: Data on microhardness for plasma nitrided specimens

Distance from surface , μm	Micro-hardness, Hv		
	Compound layer thickness, < 10 μm	Compound layer thickness >10 μm	Without compound layer
0	754	799	740
25	745	626	729
50	718	599	703
75	691	571	683

100	652	548	652
150	606	520	594
200	550	503	522
250	490	471	473
300	450	447	437
400	414	406	401
500	388	383	377
600	375	370	367
700	367	355	354
850	352	339	338
1000	344	326	324
Core	331	313	316

4.1.4 Microhardness profile for plasma nitrided specimens:

As mentioned above, the plasma nitrided specimens having compound layer thickness of $> 10 \mu\text{m}$ and $< 10 \mu\text{m}$ were also subjected to determination of microhardness profile using a microhardness tester at a load of 100g. Similar measurements were also done for plasma nitrided specimens without any compound layer. Figure 4.5 gives the corresponding plots. The total case depth of nitriding was estimated using this data. Considering 400 Hv as threshold core-hardness, a total case-depth of 400 μm was observed in almost all the three categories.

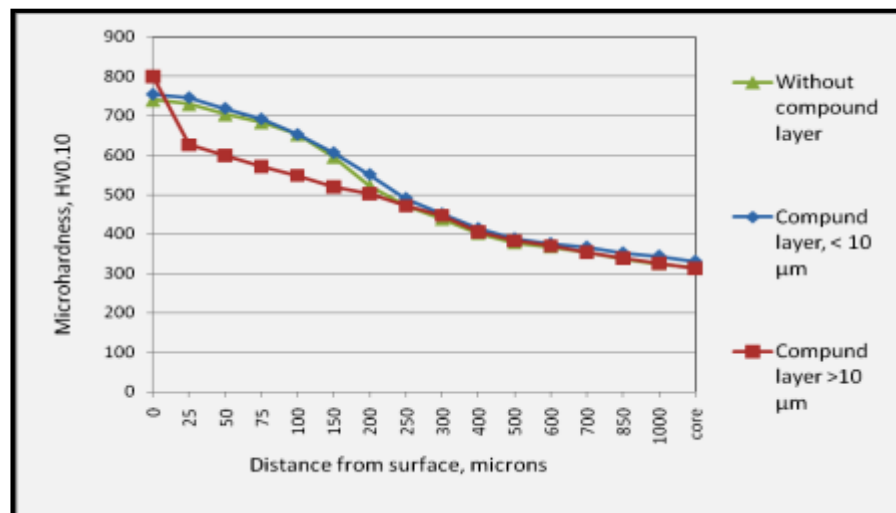


Fig. 4.5: Microhardness profile for nitrided specimens. Considering 400 Hv as threshold core-hardness, a total case-depth of 400 μm is seen in almost all the three categories.

According to Fig. 4.5 the microhardness at the surface for the specimen having higher compound layer thickness ($>10 \mu\text{m}$) is higher than that for the other two

categories. While, there is a steep decrease in the hardness below the surface for >10 μm compound layer thickness category, the hardness for the other two categories decreases gradually from surface to core as shown by a relatively smooth profile. The microhardness profile for depth greater than about 250 μm is similar for all the three categories.

This kind of microhardness profiles can be attributed to the nitrogen concentration gradient from surface (i.e. the compound layer) into the diffusion zone. When the compound layer thickness is higher, the layer is rich in nitrogen as well as nitrides formed, and so the hardness value is higher. This permits diffusion of less amount of nitrogen in the region below compound layer, and so the hardness values drop drastically below the compound layer for specimens with > 10 μm thickness of compound layer. This was confirmed by examining the nitrogen profile in diffusion layer of the plasma- nitrided specimens using EDS data (given in Appendix-I) for the element nitrogen, obtained at different locations for plasma- nitrided specimens for three different categories viz. plasma- nitrided with less than 10 microns white layer thickness, plasma- nitrided with more than 10 microns white layer thickness and plasma- nitrided but without any white layer. Figure 4.6 gives the variation in nitrogen concentration with respect to distance from nitride- layer for these conditions.

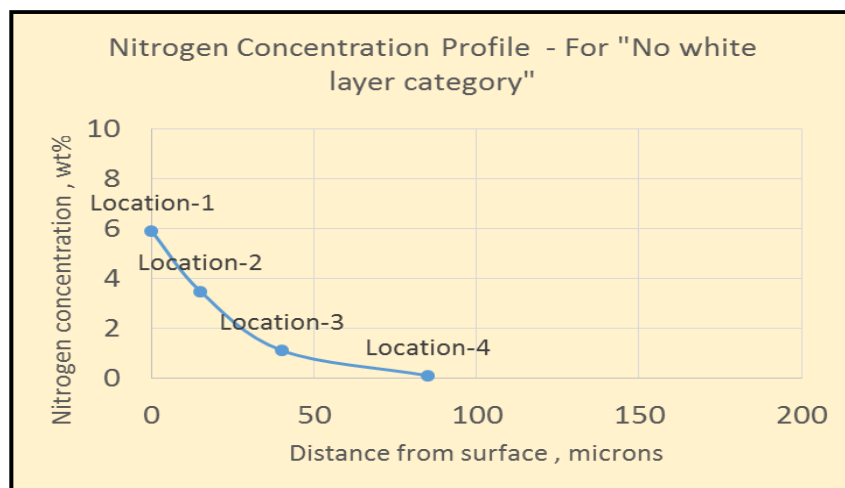


Fig. 4.6 (a): Nitrogen profile without white layer

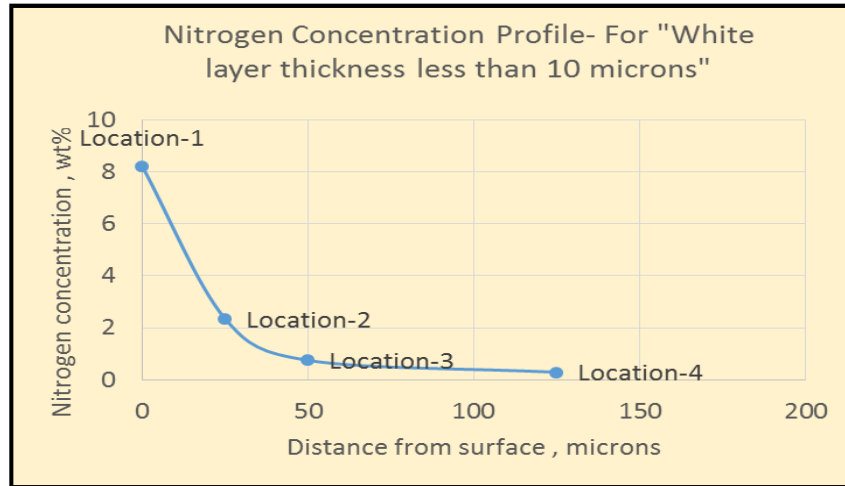


Fig. 4.6 (b): Nitrogen profile for less than 10 micron

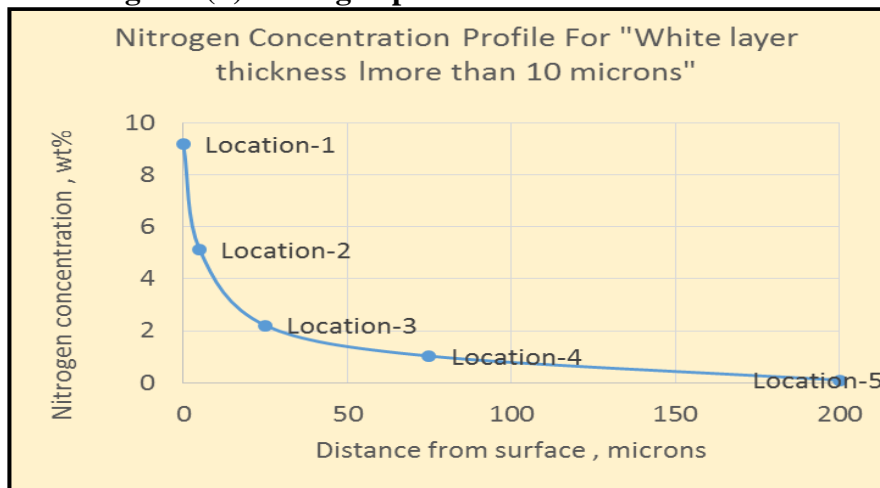


Fig. 4.6 (c): Nitrogen profile for more than 10 micron

Fig. 4.6: Variation in nitrogen concentration with respect to distance from nitrified layer for plasma- nitrified specimens

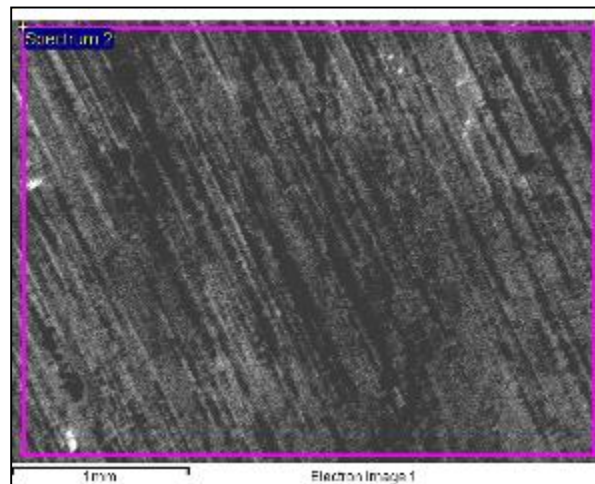
4.1.5: Compositional analysis of surface layers by EDS:

The specimens of different surface treatments were subjected to EDS analysis in order to study the composition of the coating material and the same has been given in Fig. 4.7 to 4.11. It is worth mentioning here that the analysis reported here is by and large of qualitative nature and the values for weight per cent of elements reported are not to be taken very strictly. The EDS profile for hard chrome plated specimen (Fig. 4.7) shows chromium and oxygen as the main elements present responsible for formation of chromium oxide layer. For better bonding between the alumina layer and steel substrate, a bond coat of nickel is given on steel before spraying it with alumina. This is evident in the EDS profile given in Fig. 4.8. Presence of aluminium and oxygen in major proportion in the EDS profile (Fig. 4.9) for thermal sprayed specimen confirms the presence of alumina layer in thermally sprayed specimen.

Sample: Hard chrome plated

Spectrum processing :
 Peaks possibly omitted : 1.040, 10.800 keV
 Processing option : Oxygen by stoichiometry (Normalised)
 Number of iterations = 2

Standard :
 Cr Cr 1-Jun-1999 12:00 AM
 Mn Mn 1-Jun-1999 12:00 AM



Element	Weight %	Atomic%	Compd%	Formula
Cr K	66.44	39.00	97.11	Cr ₂ O ₃
Mn K	2.24	1.24	2.89	MnO
O	31.32	59.75		
Totals	100.00			

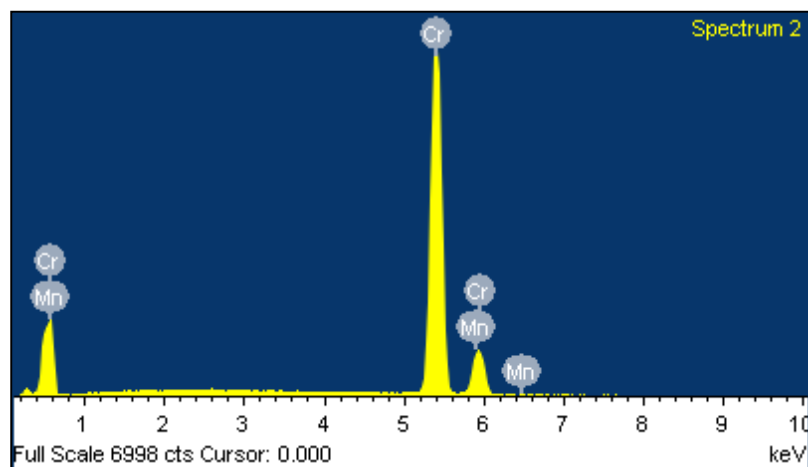


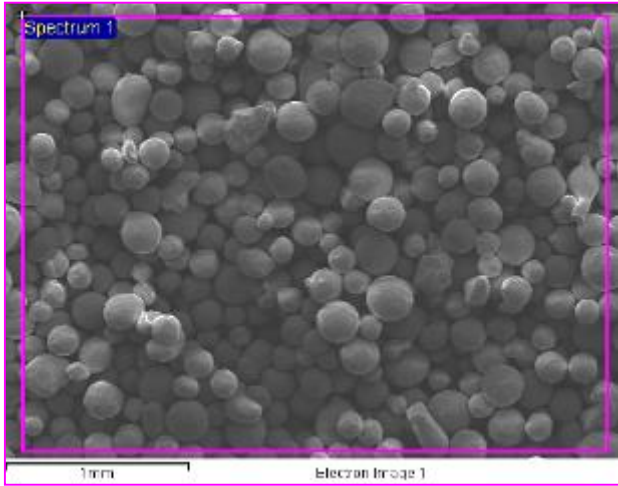
Fig. 4.7: EDS analysis of hard chrome plated specimen

Sample: Bond-coat powder for Thermal spray coating of alumina

Spectrum processing :
 No peaks omitted

Processing option : All elements analyzed
 (Normalised)
 Number of iterations = 3

Standard :
 O SiO2 1-Jun-1999 12:00 AM
 Al Al2O3 1-Jun-1999 12:00 AM
 Si SiO2 1-Jun-1999 12:00 AM
 Fe Fe 1-Jun-1999 12:00 AM
 Ni Ni 1-Jun-1999 12:00 AM
 Ta Ta 1-Jun-1999 12:00 AM



Element	Weight%	Atomic%
O K	2.31	7.47
Al K	5.61	10.76
Si K	1.14	2.09
Fe K	0.36	0.34
Ni K	89.68	79.08
Ta M	0.91	0.26
Totals	100.00	

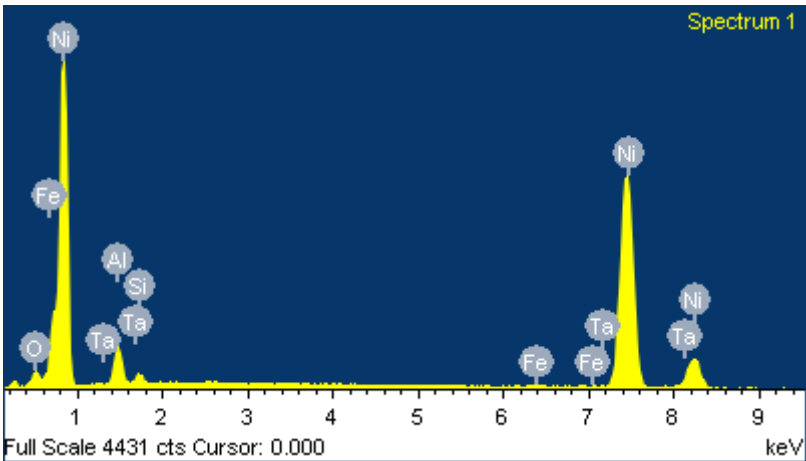


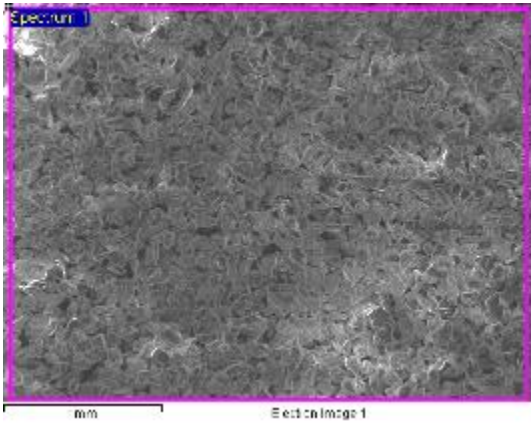
Fig. 4.8: EDS analysis of bond-coat powder for thermal spray coating of alumina

Sample: Thermally sprayed with alumina

Spectrum processing :
 Peak possibly omitted : 2.705 keV

Processing option : Oxygen by stoichiometry
 (Normalised)
 Number of iterations = 2

Standard :
 Al Al₂O₃ 1-Jun-1999 12:00 AM
 Ti Ti 1-Jun-1999 12:00 AM



Element	Weight%	Atomic%	Compd%	Formula
Al K	51.65	39.26	97.58	Al ₂ O ₃
Ti K	1.45	0.62	2.42	TiO ₂
O	46.90	60.12		
Totals	100.00			

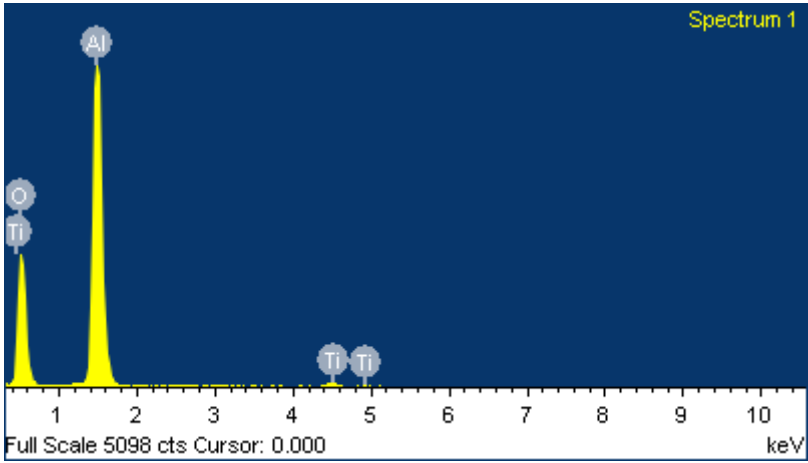


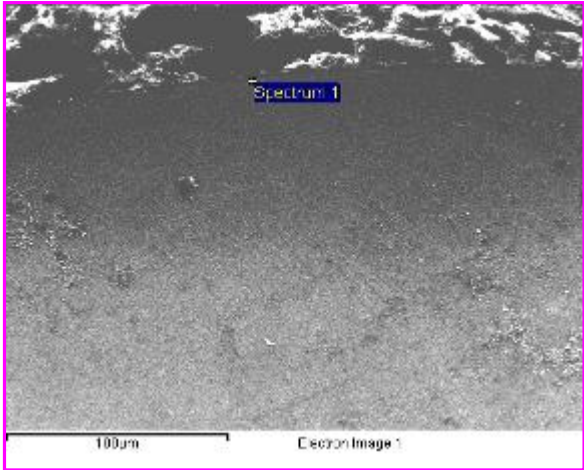
Fig. 4.9: EDS analysis of thermally sprayed with alumina specimen

Sample: Plasma nitrided - without white layer

Spectrum processing :
 No peaks omitted

Processing option : All elements analyzed
 (Normalised)
 Number of iterations = 3

Standard :
 N Not defined 1-Jun-1999 12:00 AM
 Si SiO2 1-Jun-1999 12:00 AM
 Cr Cr 1-Jun-1999 12:00 AM
 Mn Mn 1-Jun-1999 12:00 AM
 Fe Fe 1-Jun-1999 12:00 AM
 Ni Ni 1-Jun-1999 12:00 AM



Element	Weight%	Atomic%
N K	5.89	19.89
Si K	0.61	1.03
Cr K	1.34	1.22
Mn K	0.84	0.72
Fe K	89.22	75.60
Ni K	1.58	1.27
Mo L	0.52	0.26
Totals	100.00	

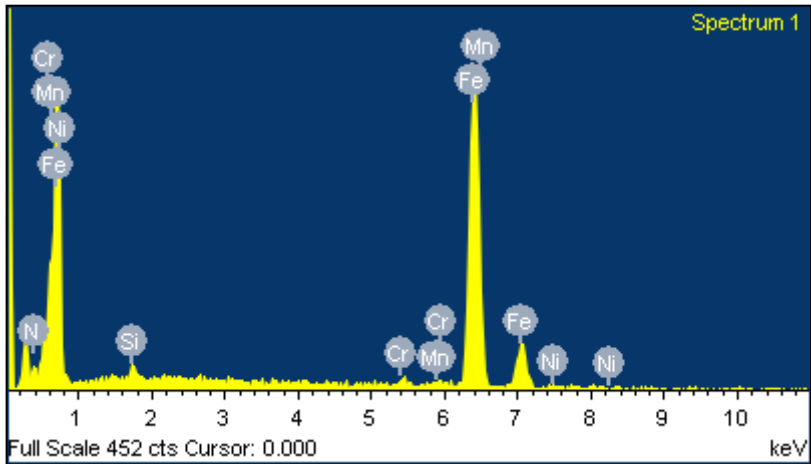


Fig. 4.10: EDS analysis of plasma nitrided specimen without white layer

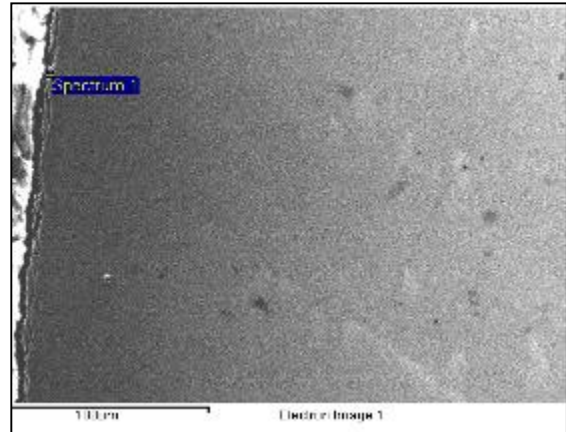
Sample: Plasma nitrided - with white layer less than 10 microns

Spectrum processing :
No peaks omitted

Processing option : All elements analyzed (Normalised)
Number of iterations = 3

Standard :

N Not defined 1-Jun-1999 12:00 AM
Si SiO2 1-Jun-1999 12:00 AM
Cr Cr 1-Jun-1999 12:00 AM
Mn Mn 1-Jun-1999 12:00 AM
Fe Fe 1-Jun-1999 12:00 AM
Ni Ni 1-Jun-1999 12:00 AM
Mo Mo 1-Jun-1999 12:00 AM



Element	Weight%	Atomic%
N K	8.22	26.24
Si K	0.46	0.73
Cr K	0.52	0.45
Mn K	0.63	0.51
Fe K	88.64	70.97
Ni K	1.32	1.01
Mo L	0.21	0.10
Totals	100.00	

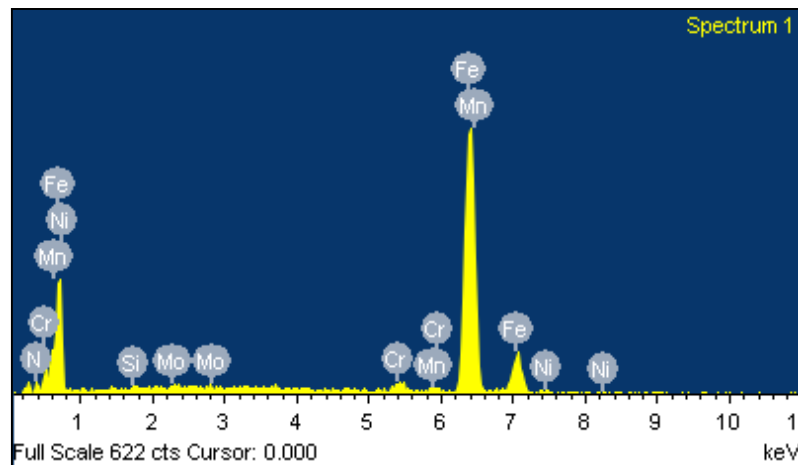


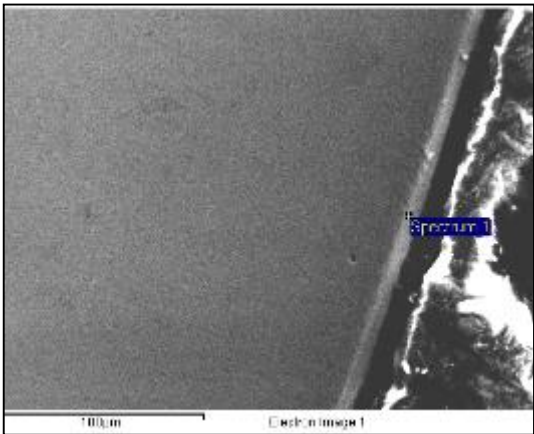
Fig. 4.11 (a) : EDS analysis of plasma nitrided specimen with white layer less than 10 microns

Sample: Plasma nitrided - with white layer more than 10 microns

Spectrum processing :
No peaks omitted

Processing option : All elements analyzed
(Normalised)
Number of iterations = 3

Standard :
N Not defined 1-Jun-1999 12:00 AM
Si SiO2 1-Jun-1999 12:00 AM
Cr Cr 1-Jun-1999 12:00 AM
Mn Mn 1-Jun-1999 12:00 AM
Fe Fe 1-Jun-1999 12:00 AM
Ni Ni 1-Jun-1999 12:00 AM
Mo Mo 1-Jun-1999 12:00 AM



Element	Weight%	Atomic%
N K	9.18	28.51
Si K	0.96	1.48
Cr K	0.81	0.68
Mn K	0.33	0.26
Fe K	87.53	68.19
Ni K	1.20	0.89
Totals	100.00	

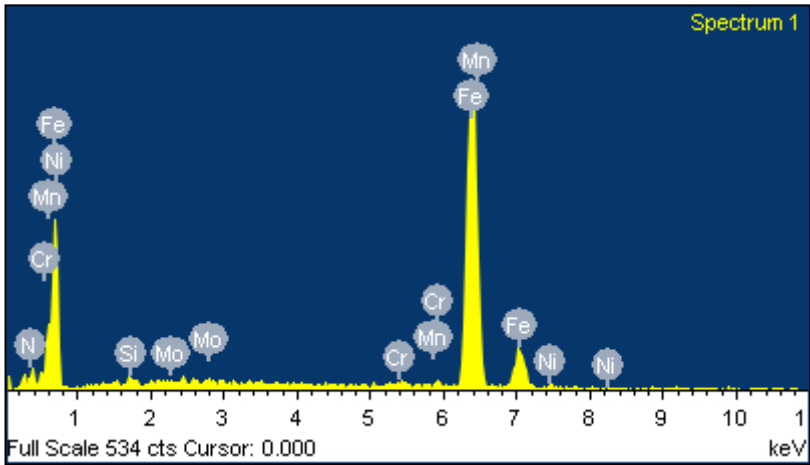


Fig. 4.11 (b) : EDS analysis of plasma nitrided specimen with white layer more than 10 microns

4.2 Post-fatigue test phase

4.2.1 Analysis of fatigue test data:

Fatigue test data generated as a result of experiments carried out as discussed in Section 3.5 have been classified and analysed as follow:

- S-N (Stress versus life cycles) data and their respective plots for each surface treatment including untreated specimen category
- S-N data converted using Basquin relationships and their respective plots
- Stress modification and Cycle modification factors calculated using above data

4.2.1.1 S-N (Stress versus life cycle) data:

The results obtained in terms of the number of cycles to failure at any given alternating stress level for the untreated specimens, hard chrome specimens, alumina sprayed and the three categories of plasma nitrided (namely having white layer > 10 um, white layer < 10 microns, & without any white layer) specimens are given in Table 4.5 to 4.10.

For obtaining S-N data from fatigue test results, the number of cycles before fracture has been considered as the criteria. In case, where fracture has not been observed for the cyclic loads applied, completion of 1.0E+08 cycles without fracture has been taken as the criteria.

Table 4.5: S-N data for base material / untreated specimens

Stress applied, MPa	No. of cycles before fracture
977	4.85E+04
907	8.48E+04
837	1.92E+05
802	2.09E+05
768	4.18E+05
698	1.00E+08*

* Sample did not break

Table 4.6: S-N data for hard chrome plated specimens

Stress applied, MPa	No. of cycles before fracture
977	3.52E+04
907	4.31E+04
837	4.60E+04
767	7.29E+04
698	1.61E+05
279	2.93E+05

Table 4.7: S-N data for thermally sprayed (with alumina) specimens

Stress applied, MPa	No. of cycles before fracture
977	1.390E+04
907	1.705E+04
837	2.045E+04
768	3.050E+04
698	3.800E+04

Table 4.8: S-N data for plasma nitrided specimens with white layer of thickness less than 10 micron

Stress applied, MPa	No. of cycles before fracture
1256	6.50E+03
977	3.52E+04
907	4.08E+05
837	4.36E+06
768	7.11E+06
698	3.98E+07

Table 4.9: S-N data for plasma nitrided specimens with white layer of thickness more than 10 micron

Stress applied, MPa	No. of cycles before fracture
977	1.03E+04
907	1.28E+04
837	1.91E+04
768	2.13E+04
698	4.77E+04

Table 4.10: S-N data for plasma nitrided specimens without any white layer

Stress applied, MPa	No. of cycles before fracture
1116	3.97E+04
1047	6.64E+04
977	2.12E+07
907	1.02E+08*
837	1.07E+08*

**Sample did not break*

4.2.1.2 Conversion of S-N data using Basquin relationship

The data given in Table 4.5 to 4.10 as generated in the fatigue testing program was used to develop Basquin plots with applied Stress in MPa (σ_a) as abscissa and no. of cycles of stress reversals as the ordinate (N_f) for each category of test specimens and the same have been reported in Fig. 4.12 to 4.17. In these plots, the predictions of the derived Basquin relationships as per Eq. 3.1 are superimposed on the experimental data. Based on the results obtained, the Basquin pre-exponents and post-exponents for

untreated and various surface treated specimens are evaluated and summarized in Table 4.11 below.

Table 4.11: Data on Basquin pre-exponents and post-exponents for untreated and various surface treated specimens

Category	Basquin Pre-exponent (α_i), MPa	Basquin Post-exponent (β_i), MPa
Base material / Untreated specimens	3.31E+03	-0.11
Hard chrome plated specimens	1.75E+05	-0.49
Thermally sprayed specimens (Alumina)	1.934E+04	-0.314
Plasma nitrided specimens (Group – I)	1.958E+03	-0.059
Plasma nitrided specimens (Group – II)	6.974E+03	-0.22
Plasma nitrided specimens (Group – III)	1.45E+03	-0.027

Where,

Group – I : With white layer of thickness <10 micron

Group – II : With white layer of thickness >10 micron

Group –III : Without any white layer

4.2.1.3 Calculation of Stress modification and Cycle modification factors

In order to determine the effect of the coating / surface treatment on the fatigue life of the base material i.e. En-24 steel in this case, the Fatigue Stress Modification Factors (FSMF), $(\theta_{coat})_I$ and the Cycle Modification Factor, Ψ_i were derived, using Equation 3.1. Figure 4.18 to 4.22 give the plots for variation in Fatigue Stress Modification Factors with respect to no. of cycles of stress reversals for untreated, thermally sprayed, and plasma nitrided specimens of three different categories.

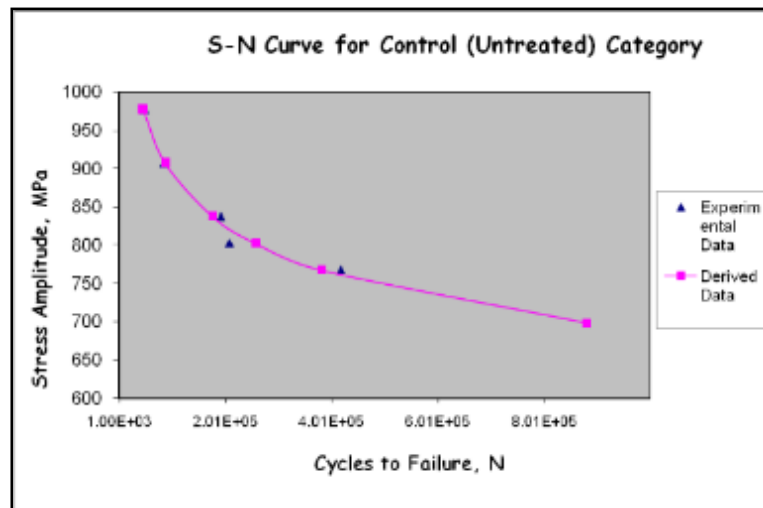


Fig. 4.12: S-N curve for base material / untreated specimens

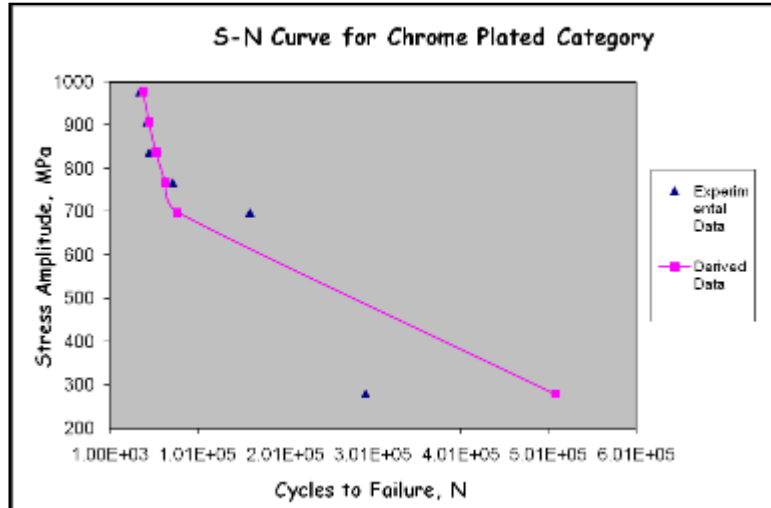


Fig. 4.13: S-N curve for hard chrome plated specimens

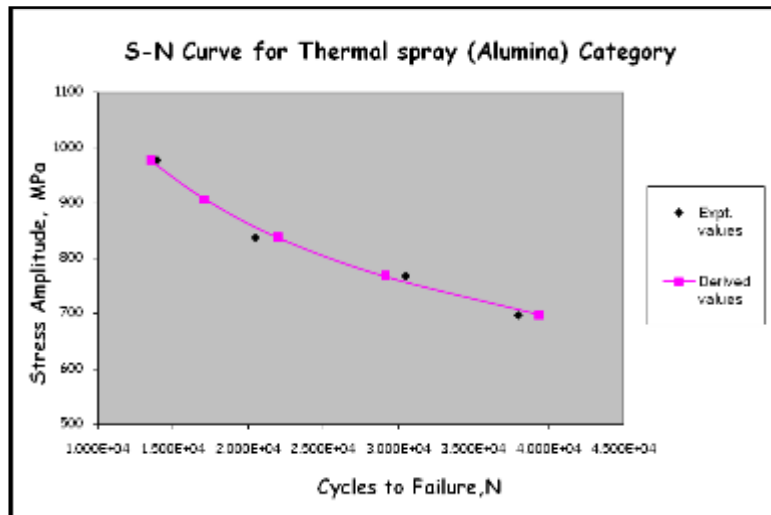


Fig. 4.14: S-N curve for thermally sprayed (with alumina) specimens

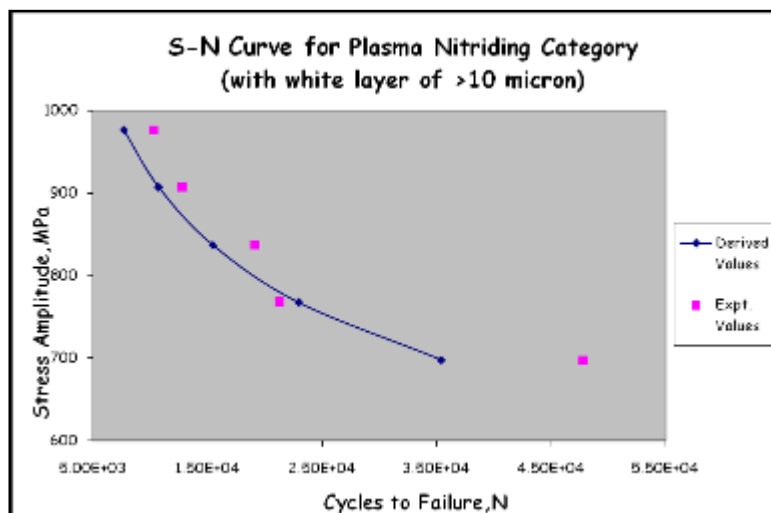


Fig.4.15: S-N curve for plasma nitrided specimens with >10 μm white layer thickness

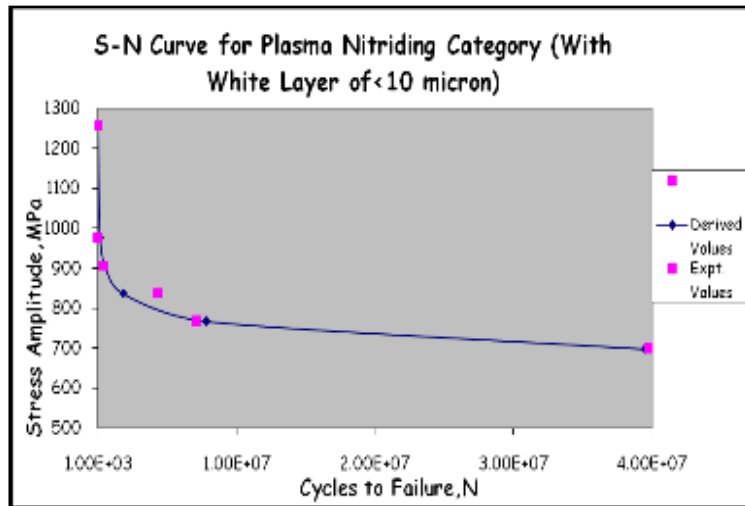


Fig.4.16: S-N curve for plasma nitrided specimens with <10 μm white layer thickness

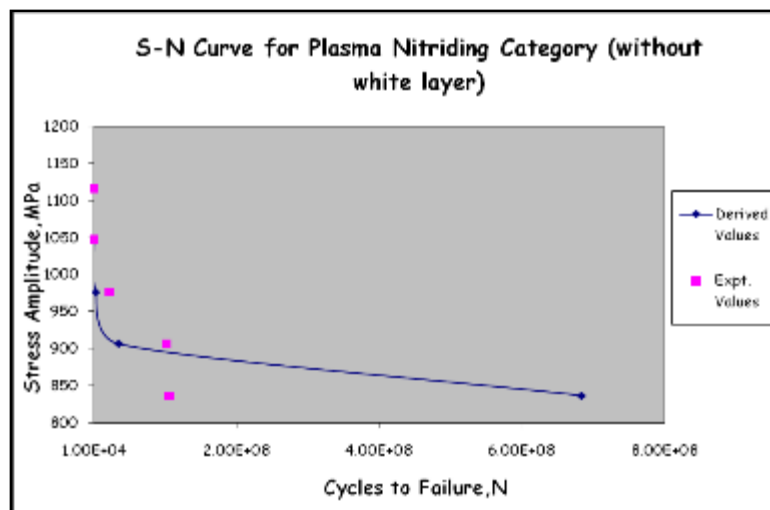


Fig.4.17: S-N curve for plasma nitrided specimens without any white layer

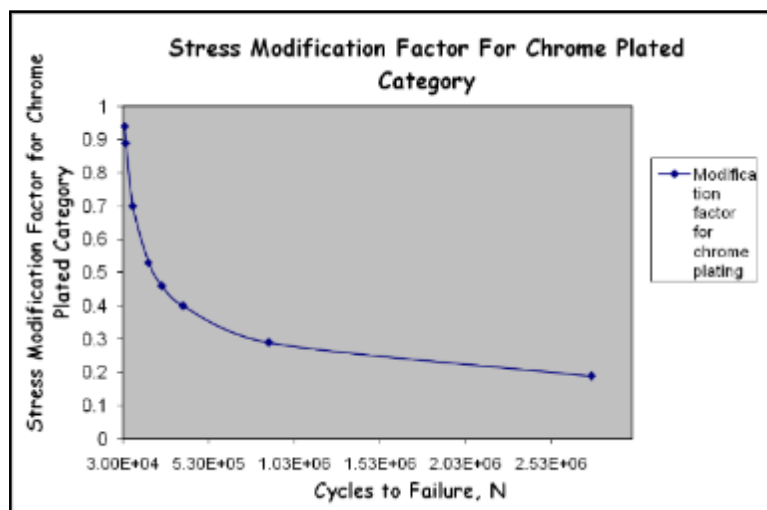


Fig. 4.18: Stress modification factor for hard chrome plated specimens is less than 1 indicating adverse effect on fatigue life.

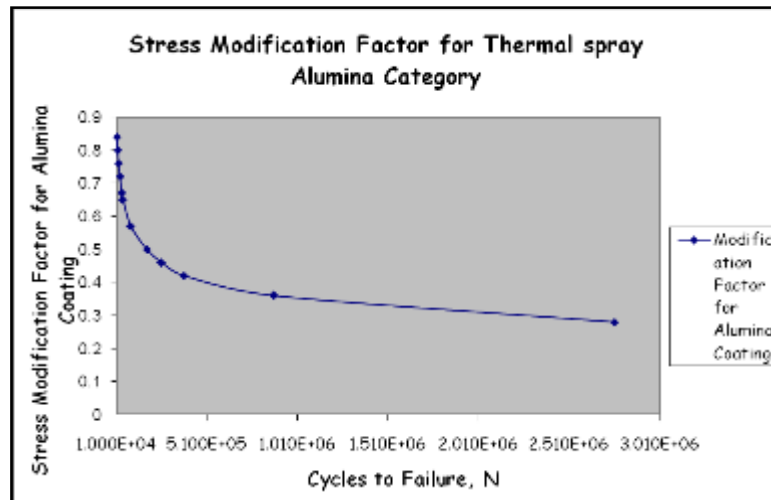


Fig. 4.19: Stress modification factor for thermally sprayed specimens is less than 1 indicating adverse effect on fatigue life.

Likewise, similar plots for variation in Cycle Modification Factors with respect to the amount of applied stress for respective specimens are given in Fig. 4.23 to 4.27.

For ease of interpretation of the effect of various surface treatments on fatigue behaviour of the steel under this investigation, the data obtained and the plots given in Fig. 4.12 to 4.27 are further discussed below on a comparative basis.

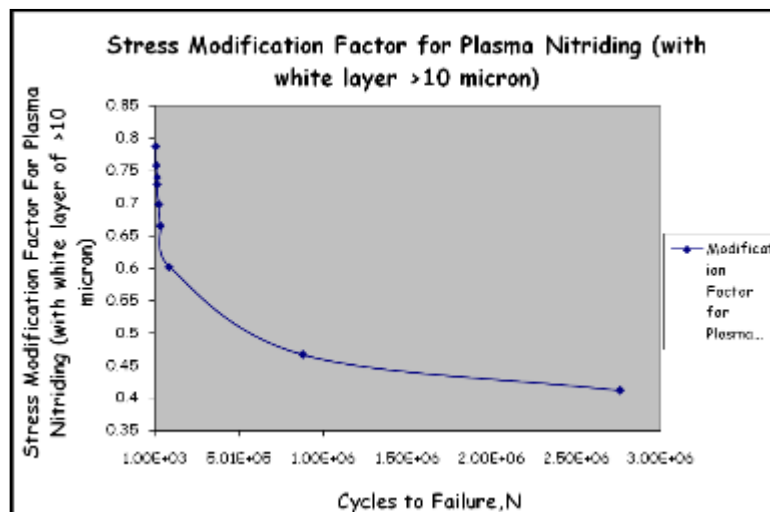


Fig. 4.20: Stress modification factor for plasma nitrided specimens with >10 μm white layer thickness is less than 1 indicating adverse effect on fatigue life.

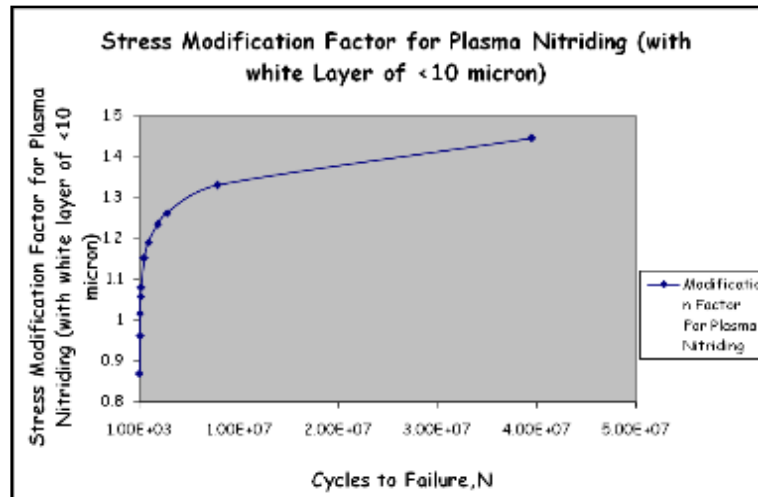


Fig. 4.21: Stress modification factor for plasma nitrided specimens with <10 μm white layer thickness, is more than 1 indicating beneficial effect on fatigue life.

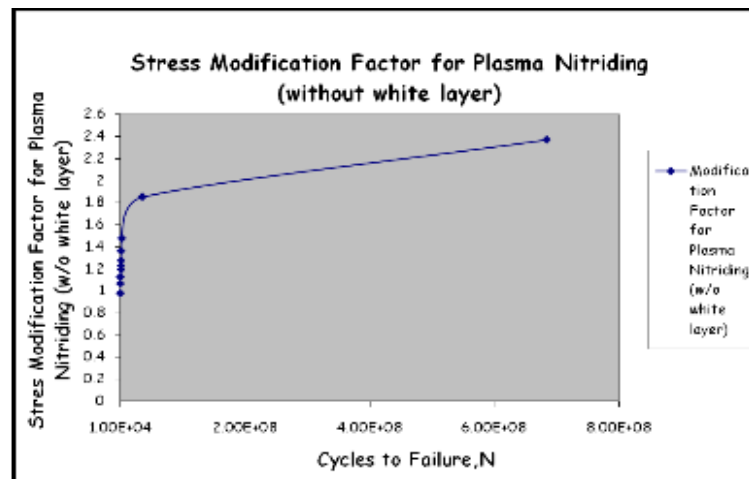


Fig. 4.22: Stress modification factor for plasma nitriding (without white layer) is more than 1 indicating beneficial effect on fatigue life.

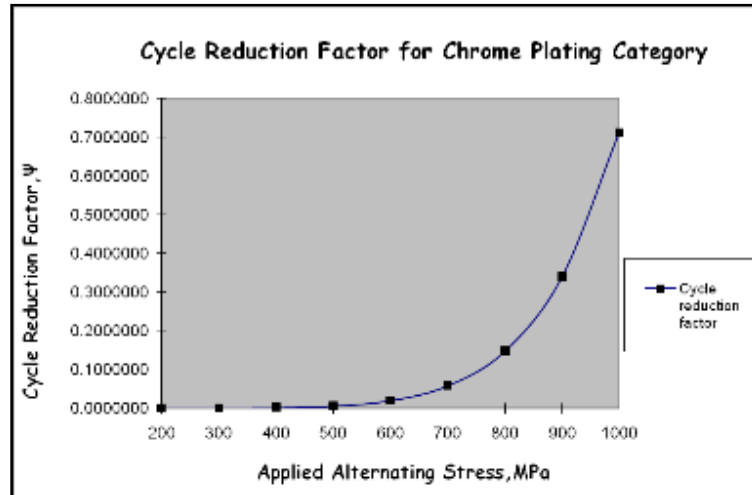


Fig. 4.23: Cycle Modification Factor for hard chrome plated specimens is less than 1 indicating adverse effect on fatigue life.

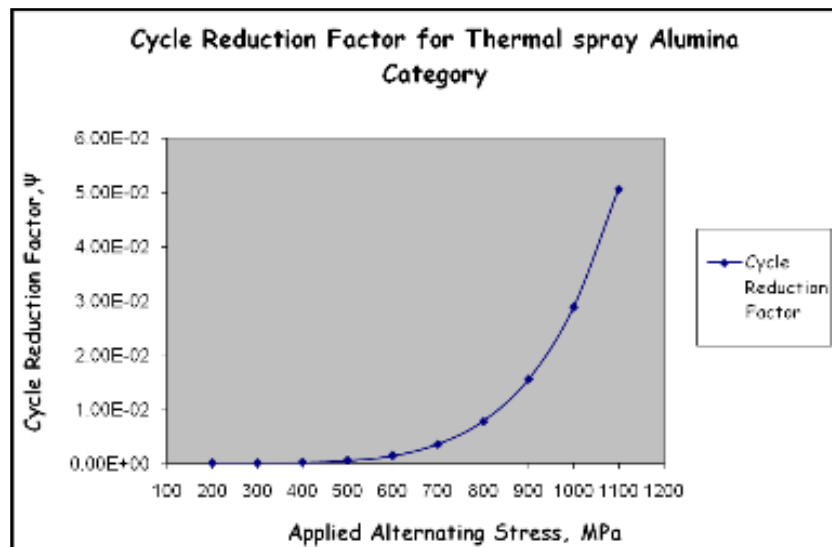


Fig.4.24: Cycle Modification Factor for thermally sprayed (with alumina) Specimens is less than 1 indicating adverse effect on fatigue life.

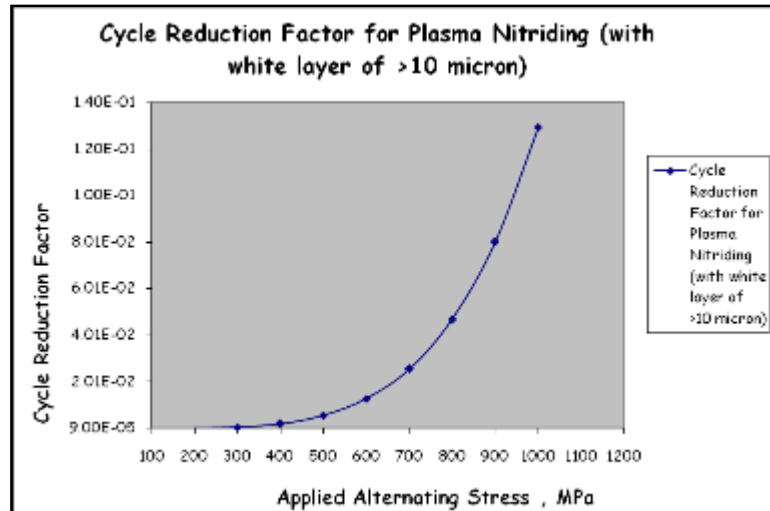


Fig. 4.25: Cycle Modification Factor for plasma nitrided specimens with >10 μm white layer thickness is less than 1 indicating adverse effect on fatigue life.

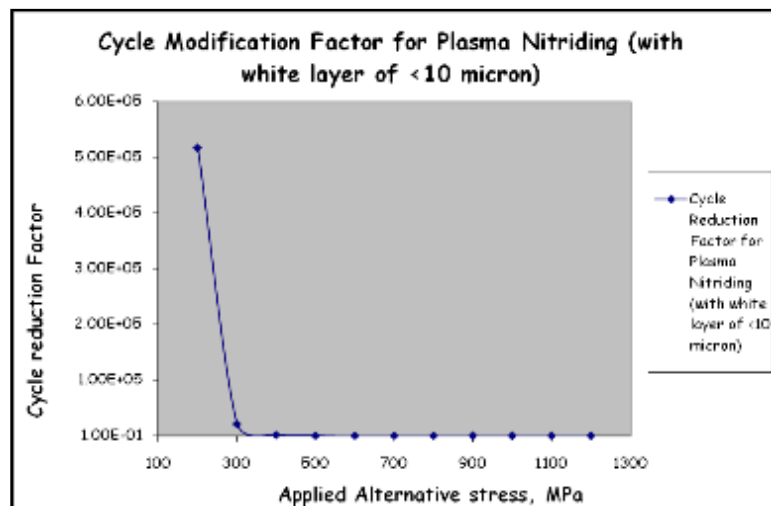


Fig. 4.26: Cycle Modification Factor for plasma nitrided specimens with <10 μm white layer of thickness is more than 1 indicating beneficial effect on fatigue life.

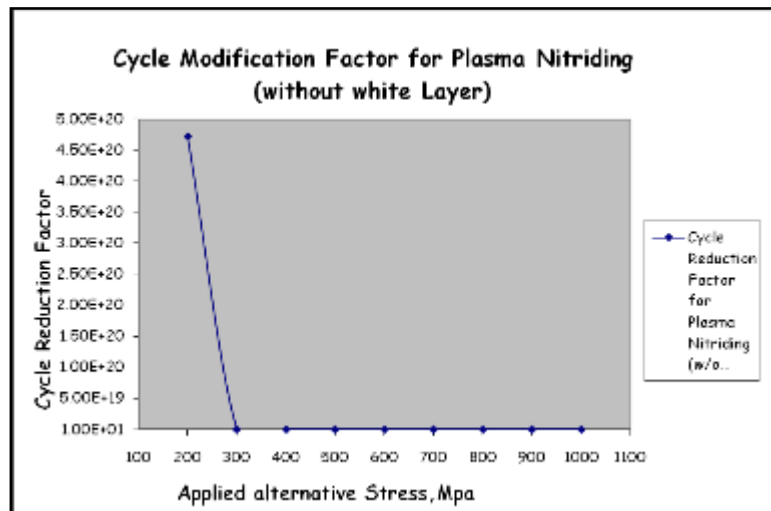


Fig. 4.27: Cycle Modification Factor for plasma nitrided specimens without any white layer is more than 1 indicating beneficial effect on fatigue life.

Fig. 4.28 and 4.29 give comparative S-N curves for untreated specimens and specimens subjected to (i) hard chrome plating, (ii) thermal spraying with alumina and (iii) plasma nitriding with $<10\ \mu\text{m}$ and $>10\ \mu\text{m}$ white layer thickness, respectively. Figure 4.28 and 4.29 clearly indicates that the maximum fatigue life is obtained in case of the specimens subjected to plasma nitriding with $<10\ \mu\text{m}$ white layer thickness and is greater than that of the untreated specimens. The fatigue life of thermally sprayed specimens and hard chrome plated specimens and plasma nitrided specimens having $>10\ \mu\text{m}$ white layer thickness is less than even un-treated specimens. In other words, these hard chrome and thermal spray treatments have an adverse effect on the fatigue behaviour of steel under consideration whereas the fatigue life of plasma nitrided steel depends on the white layer thickness.

Figure 4.30 gives an idea about the relative performance of fatigue behaviour of untreated specimens and the specimens subjected to plasma nitriding with (i) more than $10\ \mu\text{m}$, (ii) less than $10\ \mu\text{m}$ white layer thickness and (iii) without any white layer. Similar plots are given in Fig. 4.31 for S-N curves for untreated specimens and all surface treatments at a glance.

Likewise, comparative plots for stress modification factors versus no. of cycles of stress reversals are reported in Fig. 4.32 and 4.34. On similar lines the comparative plots for cycle modification factors with respect to the amount of applied stress for respective specimens are shown in Fig. 4.35 and 4.37. It is seen from these plots that

for the plasma nitrided category the maximum reduction in stress level occurs for specimens with compound layer thickness of greater than 10 μ m. For this category, the Fatigue Stress Modification Factors (FSMFs), $(\theta_{coat})_i$ are fractional (less than one), and undergo a monotonic decrease with an increase in the number of cycles to failure.

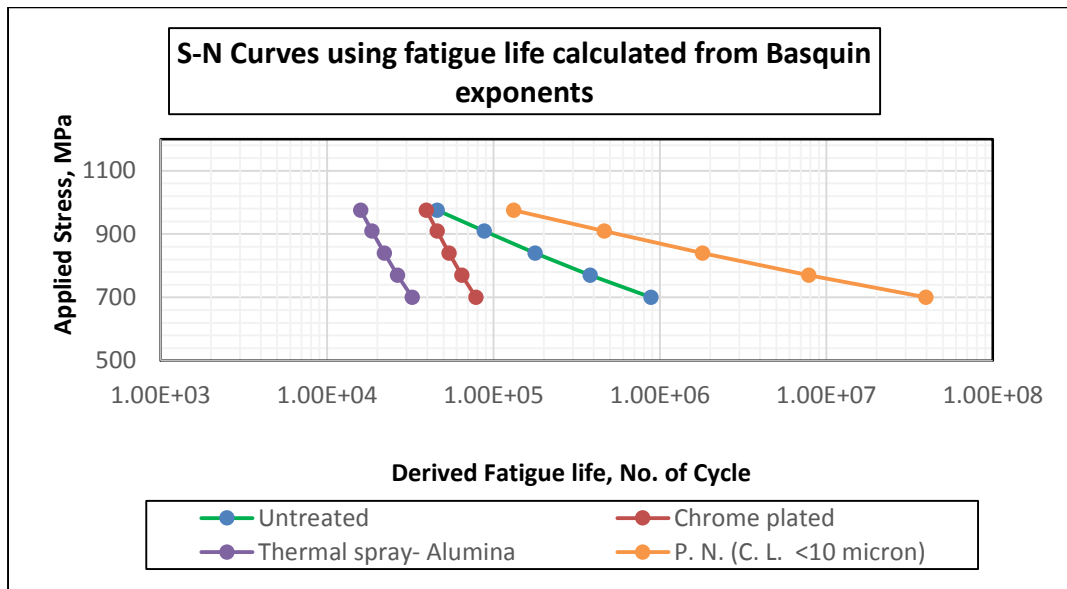


Fig. 4.28: Comparative S-N curves for untreated specimens and specimens subjected to (i) hard chrome plating, (ii) thermal spraying with alumina and (iii) plasma nitriding with <10 μ m white layer thickness. S-N curves for treatments except (iii) are on lower side as compared to untreated indicating decrease in fatigue life, while (iii) indicates increase in fatigue life.

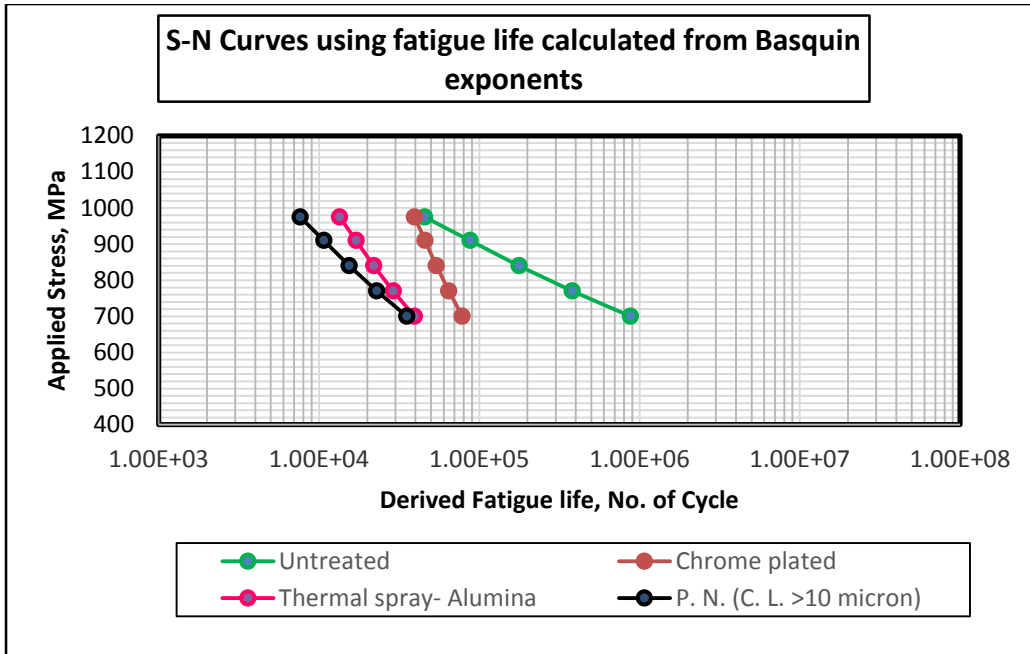


Fig. 4.29: Comparative S-N curves for untreated specimens and specimens subjected to (i) hard chrome plating, (ii) thermal spraying with alumina and (iii) plasma nitriding with >10 μm white layer thickness. S-N curves for all treatments are on lower side as compared to untreated indicating decrease in fatigue life.

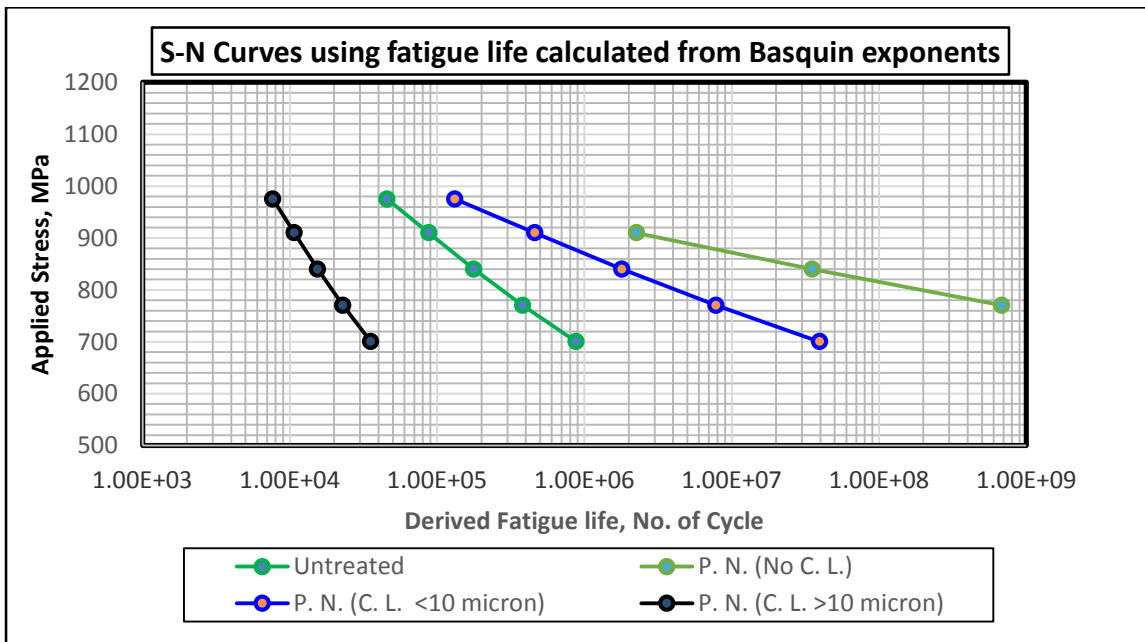


Fig. 4.30: Comparative S-N curves for untreated specimens and specimens subjected to plasma nitriding with (i) more than 10 μm , (ii) less than 10 μm white layer thickness and (iii) without any white layer. S-N curves for treatments (ii) & (iii) are on upper side compared to untreated indicating increase in fatigue life, while treatment (iii) indicates decrease in fatigue life.

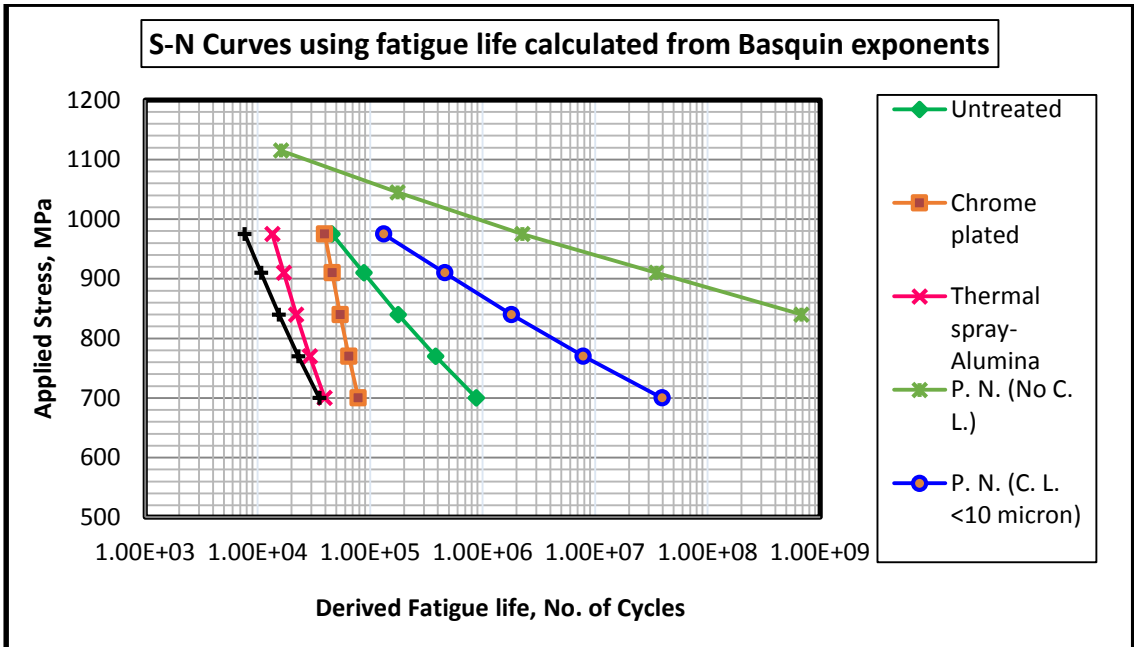


Fig. 4.31: S-N curves (Basquin plots) for specimens of untreated and all surface treatments on a comparative basis. S-N curves for two of the treatments are on upper side compared to untreated while for other three are on lower side.

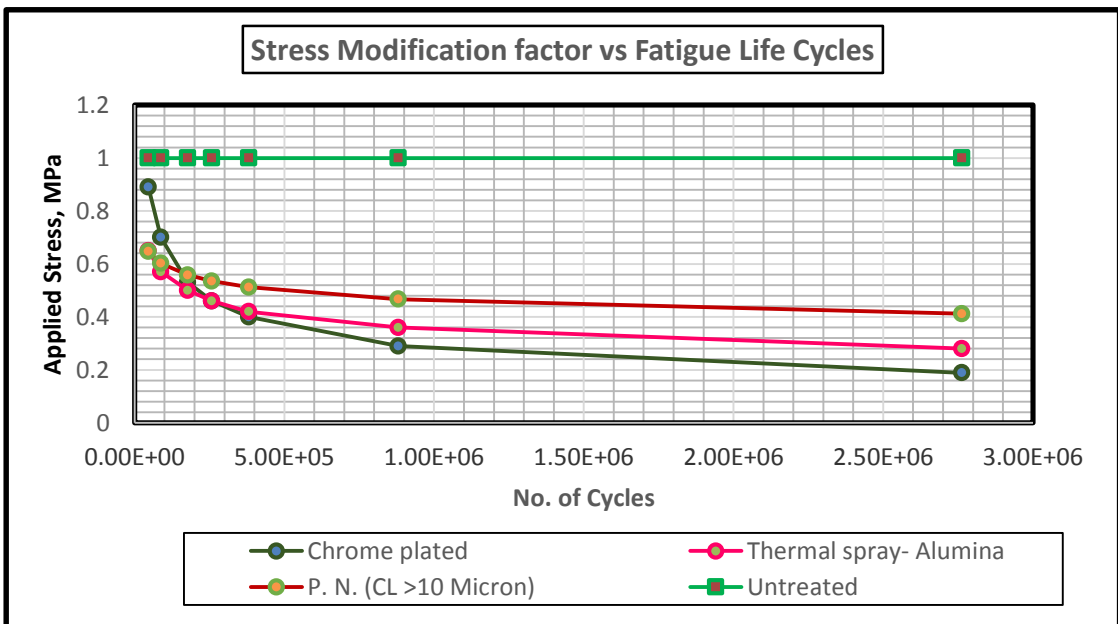


Fig. 4.32: Stress modification factor for specimens of (i) hard chrome plating, (ii) thermal spraying with alumina and (iii) plasma nitriding (with >10 μm white layer thickness) treatments on a comparative basis

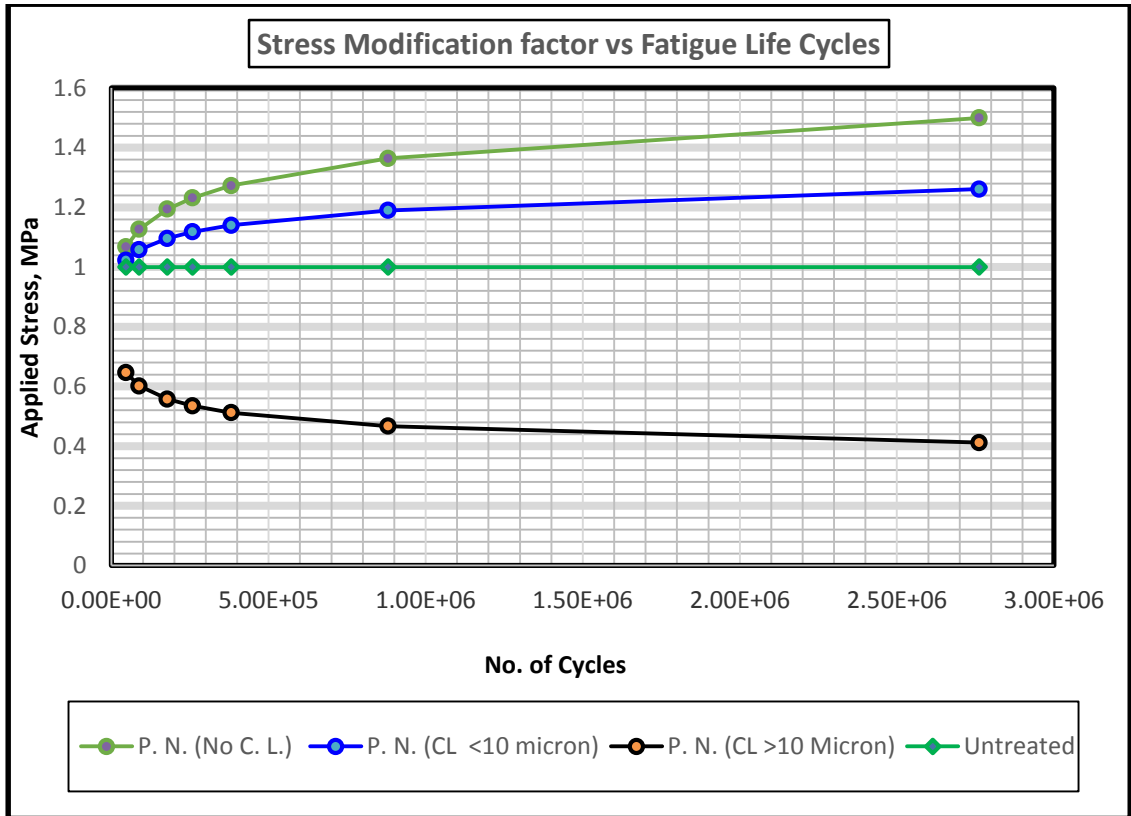


Fig. 4.33: Stress modification factor for specimens subjected to plasma nitriding with (i) more than 10 μm , (ii) less than 10 μm white layer thickness and (iii) without any white layer

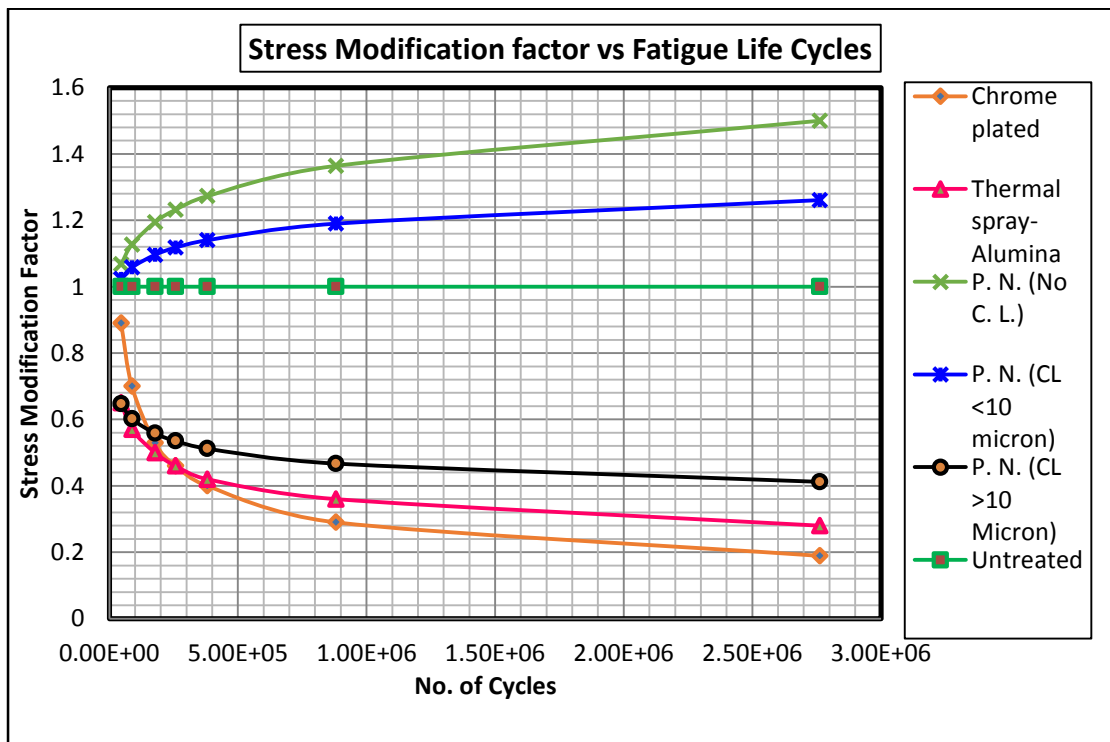


Fig. 4.34: Stress modification factor for specimens of all surface treatments on a comparative basis

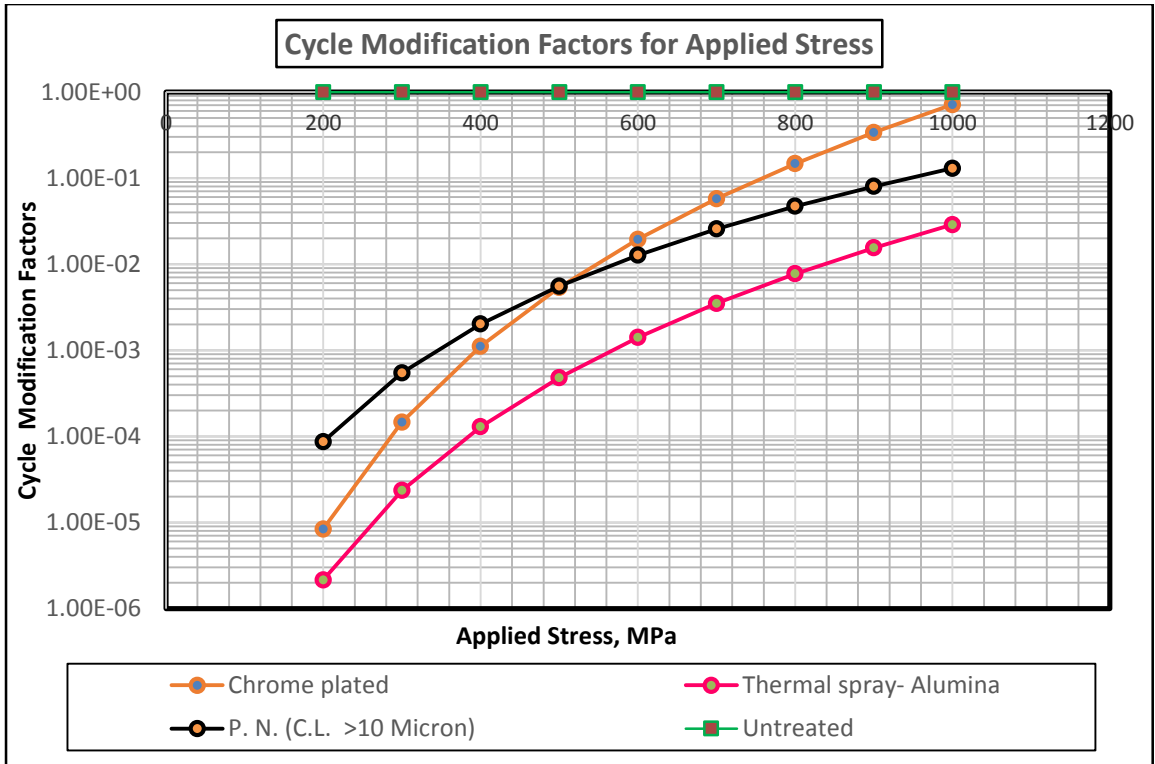


Fig. 4.35: Cycle modification factor for specimens of (i) hard chrome plating, (ii) thermal spraying with alumina and (iii) plasma nitriding (with >10 μm white layer thickness) treatments on a comparative basis

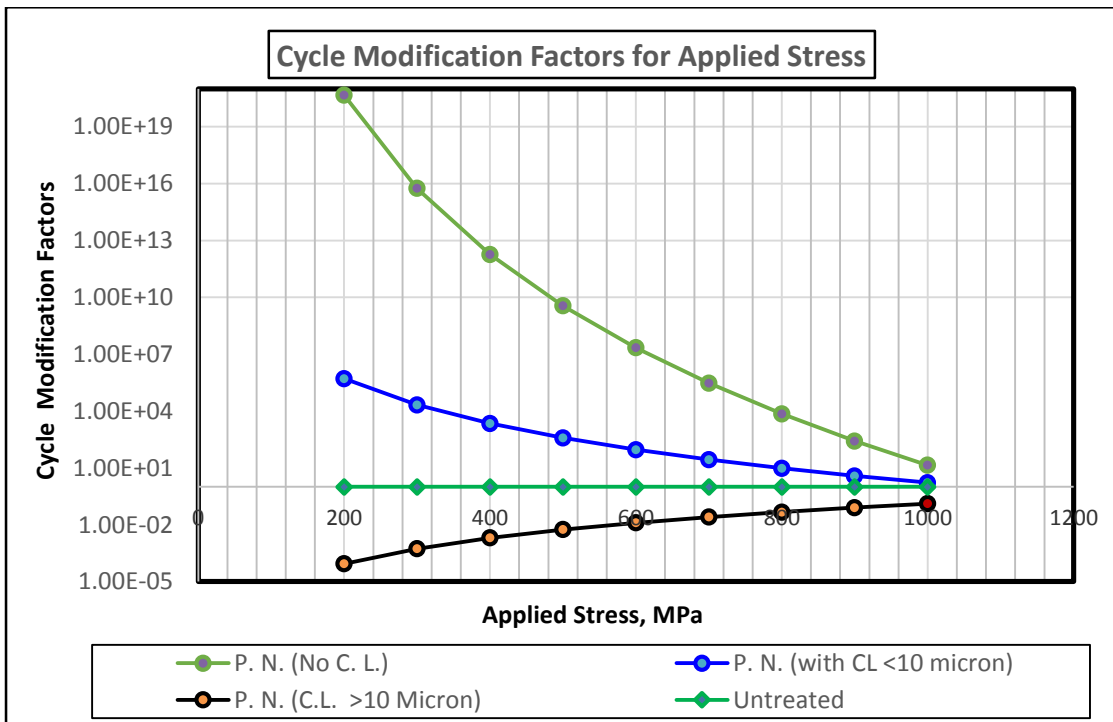


Fig. 4.36: Cycle modification factor for specimens subjected to plasma nitriding with (i) more than 10 μm , (ii) less than 10 μm white layer thickness and (iii) without any white layer

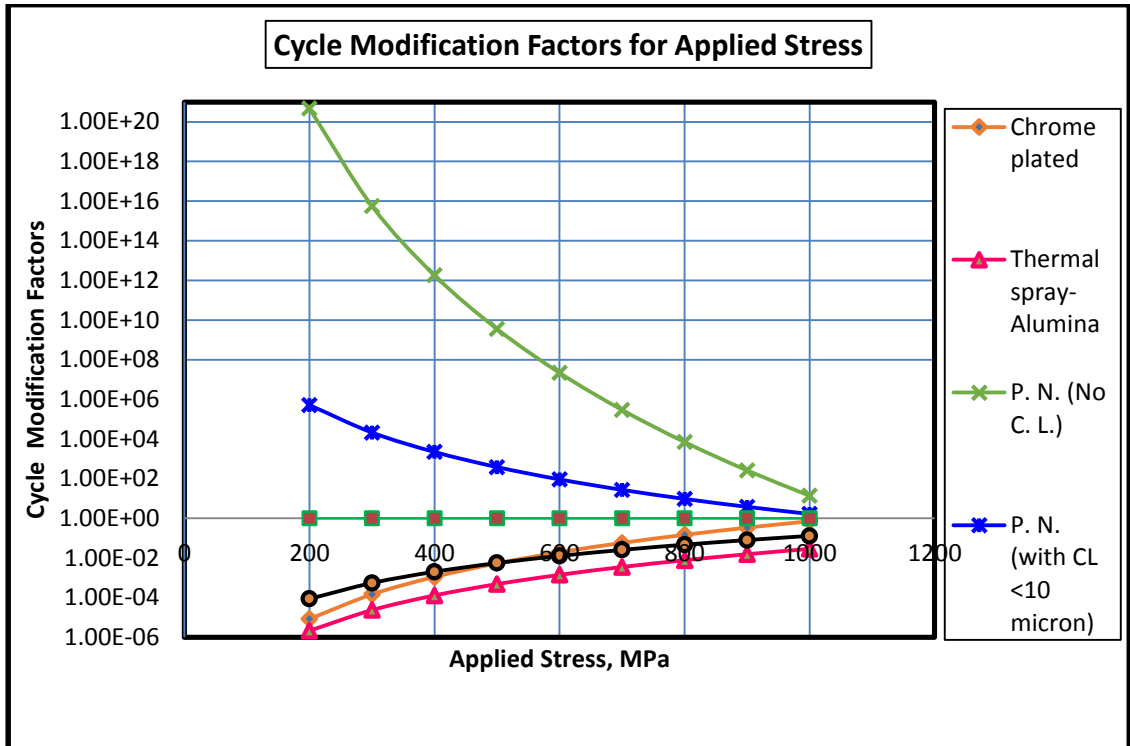


Fig. 4.37: Cycle modification factor for specimens of all surface treatments on a comparative basis

In other words, if one were to plot a superposition of the Basquin plots for this category (with thickness of compound layer greater than 10 μm) with reference to the untreated category, the Basquin plots will be translated downward, parallel to the ‘alternating stress axis’ and to the left, parallel to the ‘number of cycles to failure’ axis. The performance of specimens subjected to hard chrome plating and thermal spray coating is even worse than that of the plasma nitrided specimens with compound layer thickness of greater than 10 μm .

On the other hand, for the plasma nitrided specimens, with compound layer thickness of less than 10 μm as well as with ‘absence of compound layer’, the Fatigue Stress Modification Factors (FSMFs), $(\theta_{\text{coat}})_i$ are greater than one. The plasma nitrided category without compound layer shows the highest increase in the stress modification factor. A more critical analysis of the results also reveals that the presence of compound layer less than 10 μm is seen to degrade the fatigue resistance as compared to the fatigue resistance for the plasma nitrided category without any compound layer.

To summarize the effect of ‘stress modification factor’ on fatigue life of a component it can be said that the value of this factor indicates enhancement or reduction in fatigue life. The value of factor being equal to ‘1’ means no effect on fatigue life, i.e.

neither increase nor reduction in fatigue life. Value of factor >1 indicates enhancement in fatigue strength whereas < 1 indicates reduction in fatigue strength.

The reasons for the reduction of fatigue strength in case of hard chromium plated specimens may be several factors such as; high tensile residual stresses originated during the electrodeposition process, the parameters used in electrodeposition, the existence of microcracks in chromium, substrate hardness, the chromium plating thickness, and the strong coating / substrate interface adhesion. Hard chrome plating process leads to development of high tensile residual stresses at the surface. Literature reports that the shot peening of the surface to be subjected to hard chrome plating produces the best gain in fatigue life through the creation of Compressive Residual Stress Field (CRSF) in their surface layers. The shot peening treatment pushes the crack sources beneath the surface rather than at the surface.

The fatigue strength of nitrided components is improved by the combined effect of higher case hardness and compressive residual stresses, which result in a local endurance limit. Owing to the lower density of alloy nitrides than the iron matrix, compressive residual macro-stresses develop during nitriding. This also reduces the unfavourable factor of the notch effect which is extremely marked on fatigue limit. The growth of residual stress is caused by nitrogen being taken into solution in the matrix and the formation of nitride precipitates [2.146].

4.3 Fractography of fatigue tested specimens

The fatigue tested specimens were subjected to optical and SEM fractography to examine the fracture surface.

An important characteristic of the chromium electroplating is the high tensile residual internal stresses originated during the electrodeposition process. These high tensile stresses in electroplated chromium coatings increase as thickness increases and are relieved by local micro-cracking during electroplating. Figure 4.40 shows the fracture surface of the specimen subjected to hard chrome plating. The fracture surface shows multiple crack initiation sites at several points all along the periphery. This is confirmed by presence of multiple ratchet marks all along the periphery. The fast fracture region is small and little off-centre. The small relative size of fast fracture region with respect to fatigue zone is indicative of fracture under low-stress high-cycle conditions. The SEM micrographs given in Fig. 4.41 (a) and (b) demonstrate fatigue striations presence on the fracture surface. As against this the macrofractograph for base material /

untreated specimen subjected to fatigue testing given in Figure 4.38 does not show any peripheral ratchet marks on the fracture surface, presumably indicative of failure of the specimen due to initiation and propagation of a single crack leading to final separation. SEM micrographs given in Fig. 4.39(a) and (b) represent the microscopic features of the same specimen. Figure 4.42 and 4.43 demonstrate the multiple origin type of fracture under fatigue for the specimen subjected to alumina coating by thermal spray process. SEM micrograph given in Fig. 4.43(c) indicates crack initiation from the coating-parent metal interface.

Comparative study of fracture surfaces of plasma nitrided specimens having a white layer of $> 10 \mu\text{m}$, $< 10 \mu\text{m}$ thickness and without white layer (Figures 4.44 to 4.49) reveals that there are number of ratchet marks on the fracture surface of specimen with white layer thickness of $> 10 \mu\text{m}$ whereas it is not so for the other two. Not only this micro-cavities are seen in the white layer of the former whereas there are no such cavities in case of the latter. The crack initiation in case of the plasma nitrided specimens having a white layer of $< 10 \mu\text{m}$ thickness appears to be from the interface between the white layer and the diffusion zone as shown in Fig. 4.47 (b).

A plasma nitrided sample can be considered as a composite; in which the surface layer is hard while the core is ductile. Crack initiation on a nitrided surface exposed to maximum load requires higher stresses; therefore a crack initiates below the nitrided layer and propagates towards the core, by a "fish eye" phenomenon. Increasing the case depth can be viewed as effectively moving the fatigue crack initiation site further into the core. It means that greater applied bending stress will be required at the surface to create a sufficiently high level of stress at the case-core interface to initiate failure [2.99].

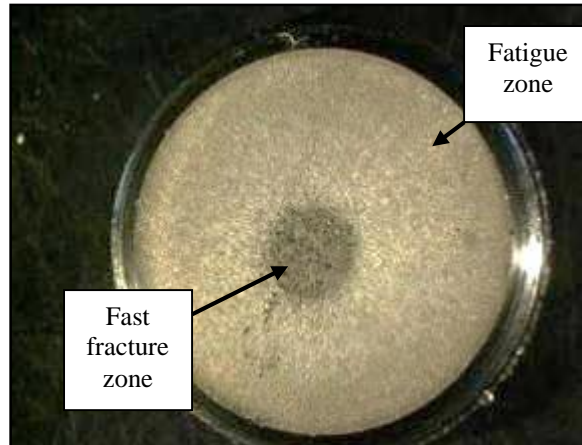


Fig. 4.38: Macrofractograph of fatigue tested untreated /base material specimen does not show any peripheral ratchet marks on the fracture surface, presumably indicative of failure of the specimen due to initiation and propagation of a single crack leading to final separation.

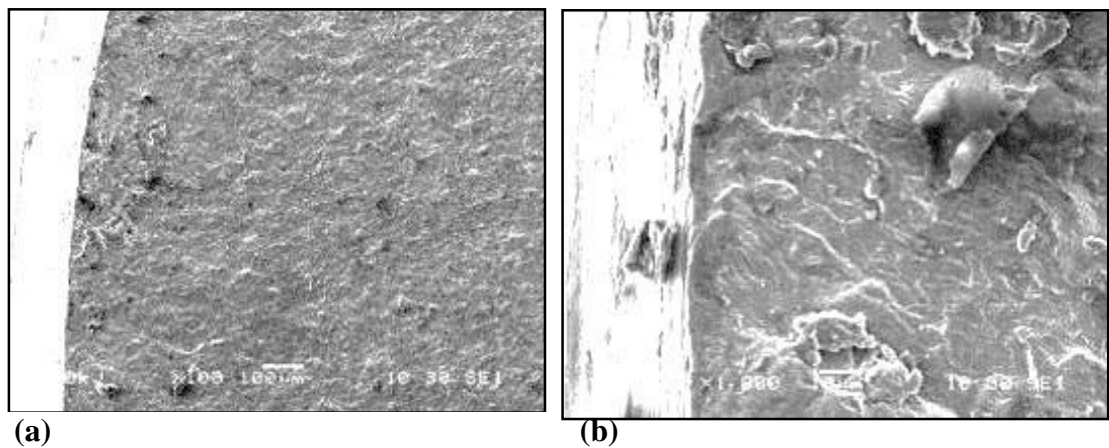


Fig. 4.39: SEM fractographs of fatigue tested untreated /base material specimen at (a) 100x and (b) 1000x magnification. Fatigue striations are seen at higher magnification.

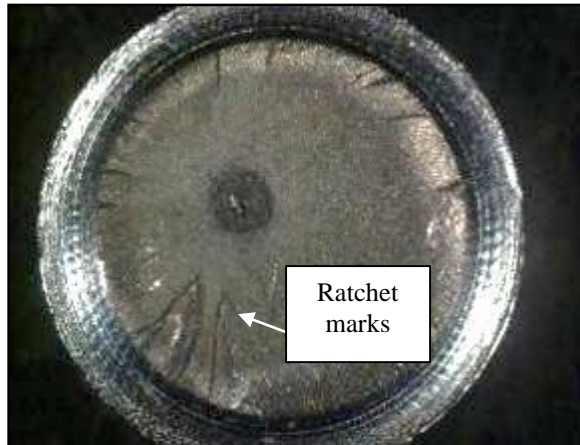


Fig. 4.40: Macrofractograph of fatigue tested hard chrome plated specimen demonstrate the multiple origin type of fracture under fatigue.

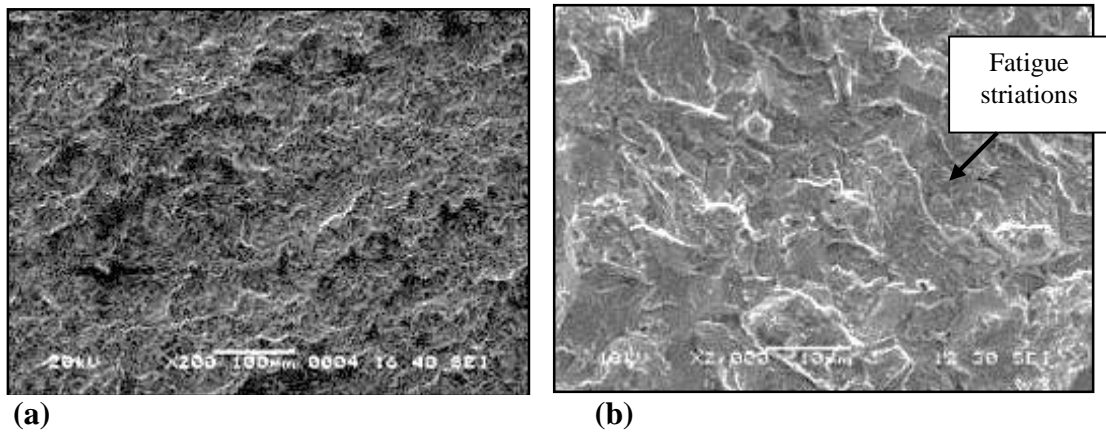


Fig. 4.41: SEM fractographs of fatigue tested hard chrome plated specimen at (a) 200x and (b) 2000x magnification. Fatigue striations are seen at higher magnification.



Fig. 4.42: Macrofractograph of fatigue tested thermally sprayed specimen demonstrate the multiple origin type of fracture under fatigue.

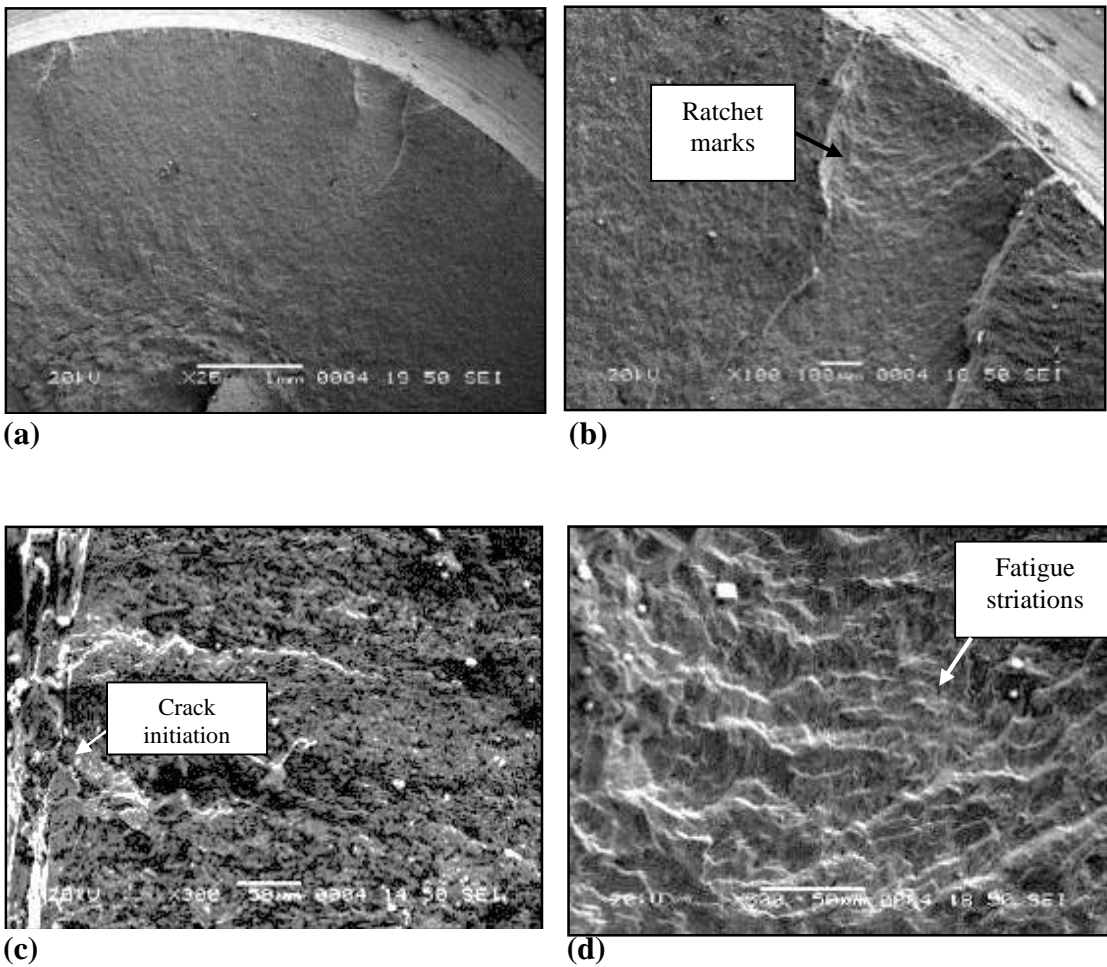
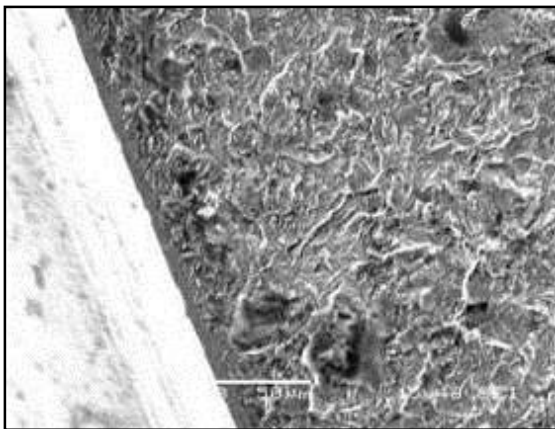


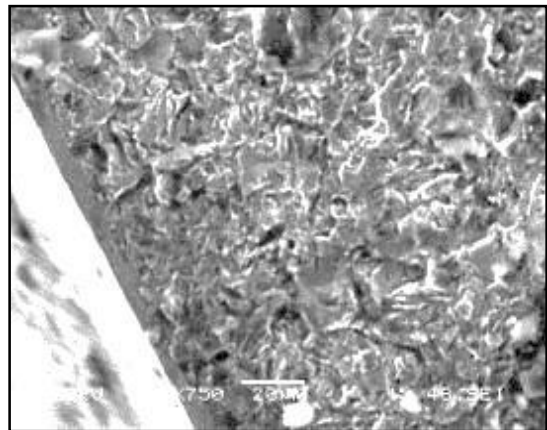
Fig. 4.43: SEM fractographs of fatigue tested thermally sprayed specimen at (a) 25x, (b) 100x, (c) 300x and (d) 500x magnification. Crack initiation & fatigue striations are seen at higher magnification.



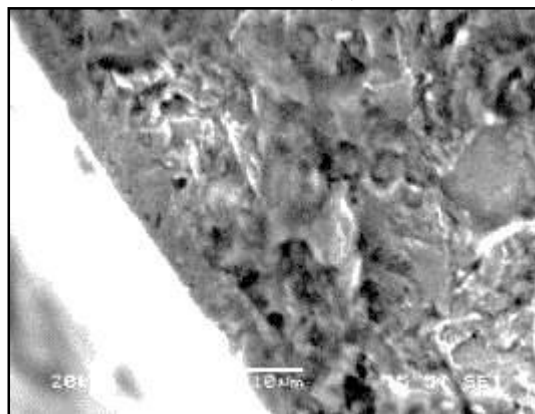
Fig. 4.44: Macrofractograph of fatigue tested plasma nitrided specimen with $> 10 \mu\text{m}$ white layer thickness demonstrate the multiple origin type of fracture under fatigue.



(a)



(b)



(c)

Fig. 4.45: SEM fractographs of fatigue tested plasma nitrided specimen with a white layer thickness of $> 10 \mu\text{m}$ at (a) 200x, (b) 700x and (c) 1000x magn. Micro-cavities are seen in the white layer.



Fig. 4.46: Macrofractograph of fatigue tested plasma nitrided specimen with $< 10 \mu\text{m}$ white layer thickness does not show any peripheral ratchet marks on the fracture surface, presumably indicative of failure of the specimen due to initiation and propagation of a single crack leading to final separation

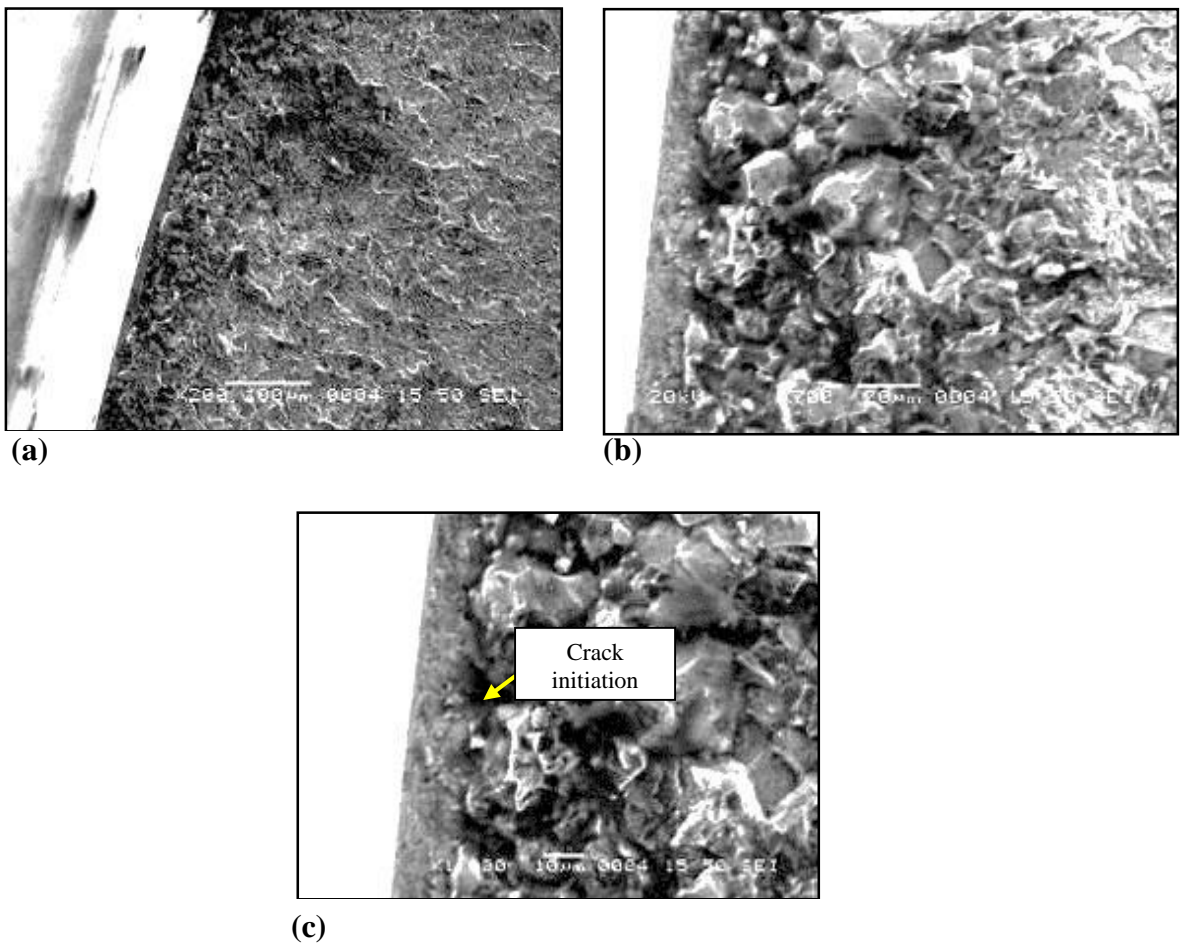
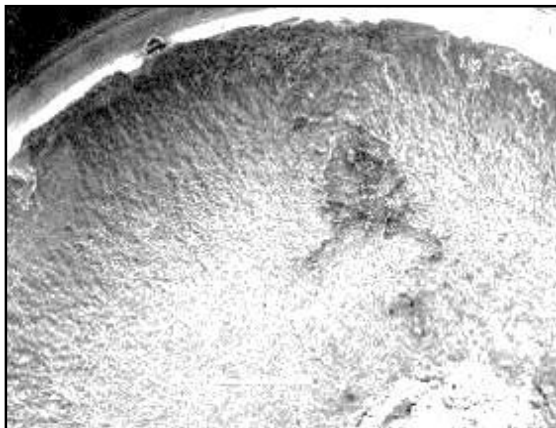


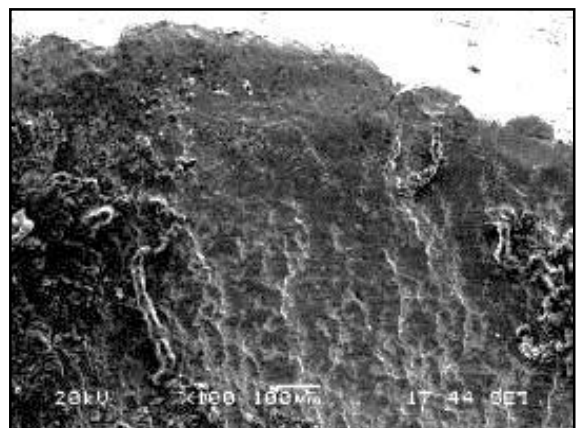
Fig. 4.47: SEM fractographs of fatigue tested plasma nitrided specimen with a white layer thickness of $< 10 \mu\text{m}$ at (a) 200x, (b) 700x and (c) 1000x magn. The crack initiation is seen to be from the interface between the white layer and the diffusion zone.



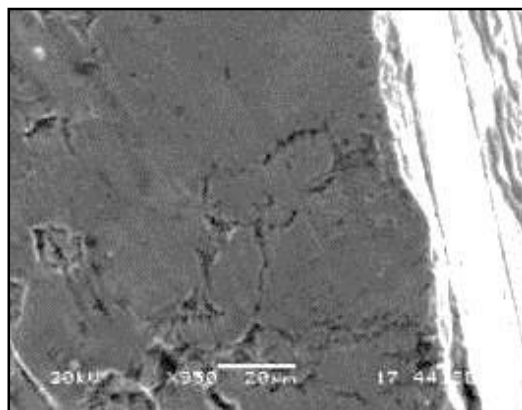
Fig. 4.48: Macrofractograph of fatigue tested plasma nitrided specimen without any white layer does not show any peripheral ratchet marks on the fracture surface, presumably indicative of failure of the specimen due to initiation and propagation of a single crack leading to final separation.



(a)



(b)



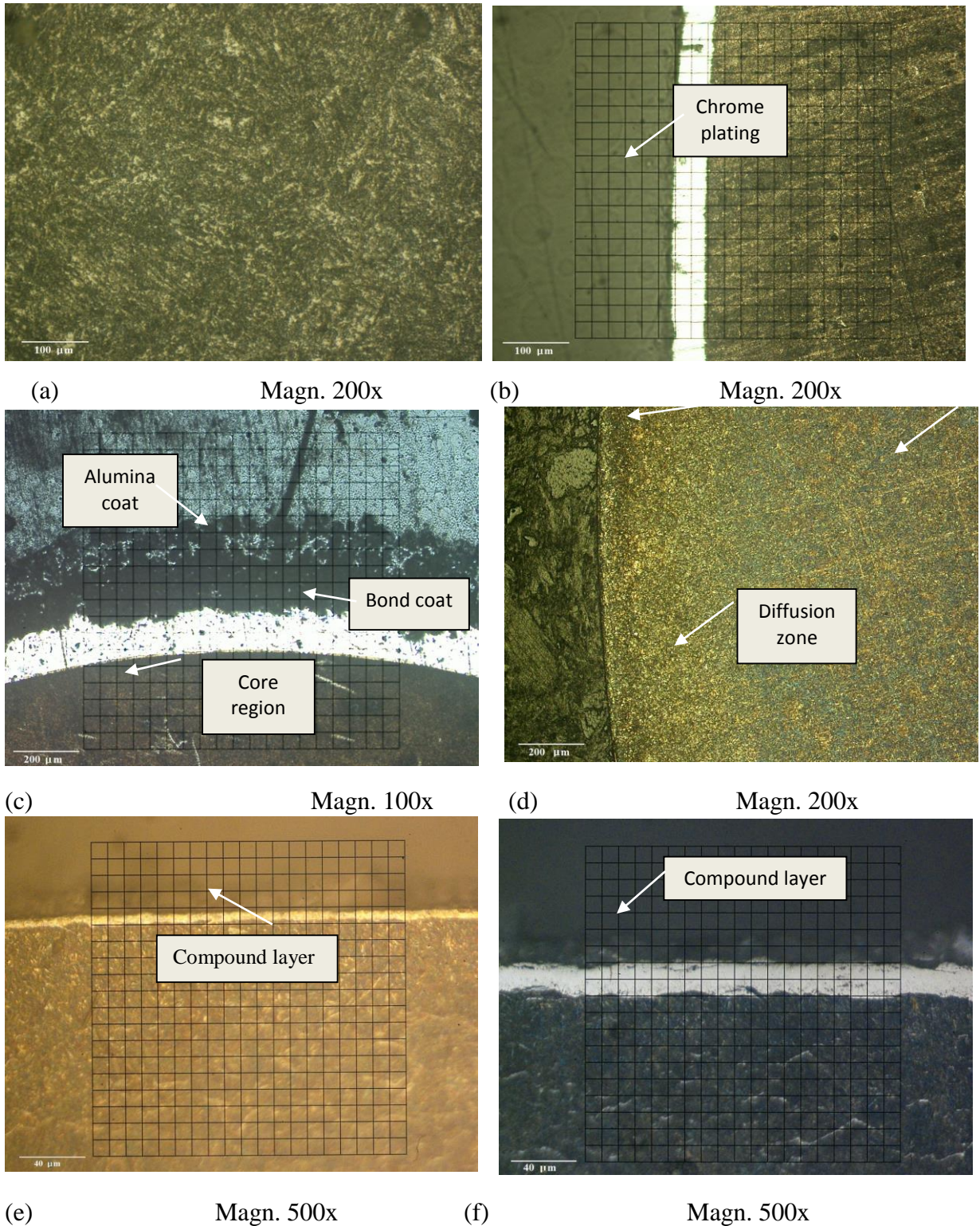
(c)

Fig. 4.49: SEM fractographs of fatigue tested plasma nitrided specimen without any white layer at (a) 25x, (b) 100x and (c) 950x magnification

4.4 Microstructural examination

Figure 4.50 shows the microstructures of base material / untreated specimen and various surface treated specimens. The microstructure of base material / untreated specimen given in Fig. 4.50(a) consist of tempered martensite with trace of retained austenite. This is the normal structure for En-24 steel in hardened and tempered condition.

Figure 4.50(b) and (c) display the presence of chromium oxide and alumina along with nickel bond coat layer on steel substrate for hard chrome plated and thermally sprayed specimens, respectively. The microstructure of base material in both the cases is tempered martensite. Photomicrographs given in ig. 4.50(d) to (f) are for specimens subjected to plasma nitriding treatment. The white layer as well as the microstructures of diffusion zone and core region are clearly marked over the images.



(e) Magn. 500x (f) Magn. 500x
 (Scale for grid – For Magn. 200x One division = 25 μm , For Magn. 500x One division = 10 μm)

Fig. 4.50: Microstructures at surface region after various treatments

- (a) Untreated / base material shows tempered martensitic structure.
- (b) Hard chrome plated shows chrome plating layer on surface.
- (c) Thermally sprayed - alumina coating shows bond coat & alumina coat
- (d) Plasma nitrided (without compound layer) – Only diffusion layer is seen
- (e) Plasma nitrided (with <10 μm white layer thickness)
- (f) Plasma nitrided (with >10 μm white layer thickness)

4.5 XRD analysis

Plasma nitrided specimens and the untreated specimen were subjected to X-Ray diffraction studies in order to identify the phases present in each case. For plasma nitrided specimens emphasis has been laid on determination of presence or absence of the γ -Fe₄N and ϵ -Fe_{2,3}N phases in compound layer. Figure 4.51 to 4.54 show the XRD profiles for the same. The XRD profiles for base material / untreated specimen and plasma nitrided specimens free from any white/compound layer show diffraction peaks corresponding to alpha iron only and as expected there are no peaks for iron nitrides /carbonitrides (Fig. 4.51& 4.52). XRD profile for plasma nitrided specimen having compound layer thickness of less than 10 μ m shows presence of diffraction peaks for Fe₄N as well as Fe₃N over and above the usual alpha iron phase (Fig. 4.53). On the other hand the XRD profile for plasma nitrided specimen having compound layer thickness of more than 10 μ m shows presence of diffraction peaks for Fe₄N and alpha iron phase as given in Fig. 4.54.

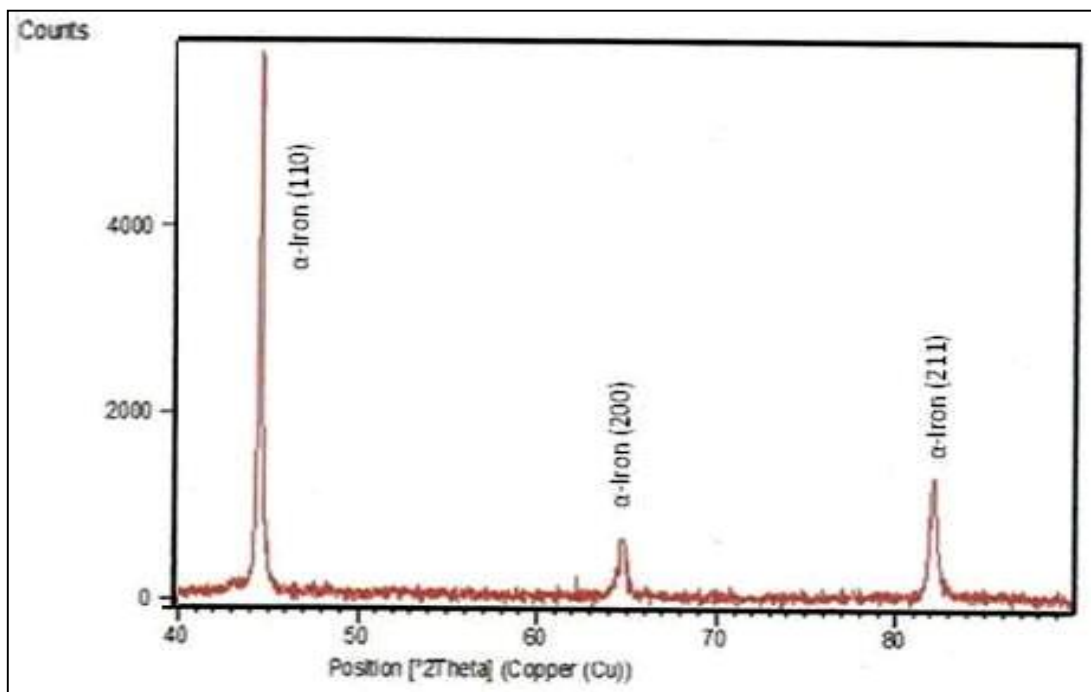


Fig. 4.51: X-ray diffraction (XRD) profile for untreated sample shows peaks of α -iron only.

Peak search results:

Sr.No.	2-Theta	Relative intensity I / I ₀	Observed 'd' value	'd' value for standard sample	Plane (hkl)
1	44.6250	100.00	2.02893	2.0268	110
2	64.9376	11.17	1.43487	1.4332	200
3	82.1104	20.60	1.17283	1.1702	211

*JCPDS File No. 6-06 96

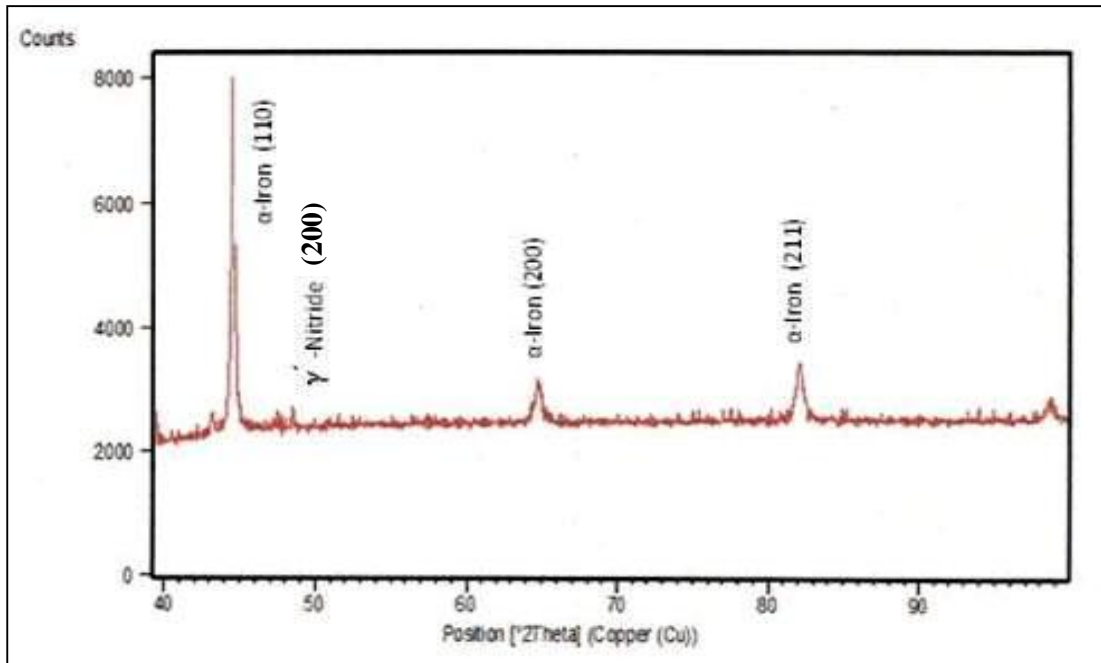


Fig. 4.52: X-ray diffraction (XRD) profile for plasma nitrided sample without compound layer shows peaks of α -iron as well as γ' -iron.

Peak search results:

Sr. No.	2-Theta	Relative intensity I / I ₀	Observed 'd' value	'd' value for standard sample	Plane (hkl)	Phase	JCPDS File No.
1	44.5775	100.00	2.03098	2.0268	110	α -Iron	6-06 96
2	47.5990	3.65	1.90887	1.897	200	γ' Iron Nitride	6-0627
3	64.7835	11.89	1.43792	1.4332	200	α -Iron	6-06 96
4	82.1230	17.74	1.17268	1.1702	211	α -Iron	6-06 96

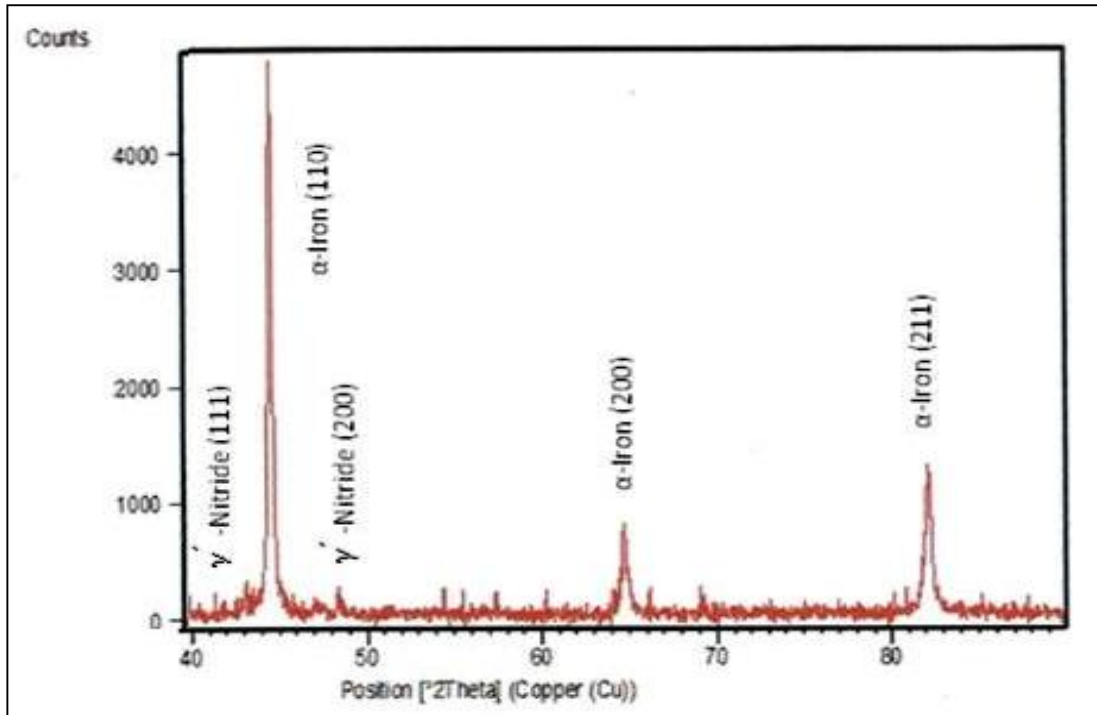


Fig. 4.53: X-ray diffraction (XRD) profile for plasma nitrided sample with compound layer thickness less than 10 microns shows peaks of α -iron as well as γ '-iron.

Peak search results:

Sr. No.	2-Theta	Relative intensity I / I _o	Observed 'd' value	'd' value for standard sample	Plane (hkl)	Phase	JCPDS File No.
1	41.42	3.27	2.17840	2.191	111	γ Iron Nitride	6-0627
2	44.598	100.00	2.03010	2.0268	110	α -Iron	6-06 96
3	47.36	1.46	1.91811	1.897	200	γ Iron Nitride	6-0627
4	64.80	11.17	1.43753	1.4332	200	α -Iron	6-06 96
5	82.175	20.60	1.17207	1.1702	211	α -Iron	6-06 96

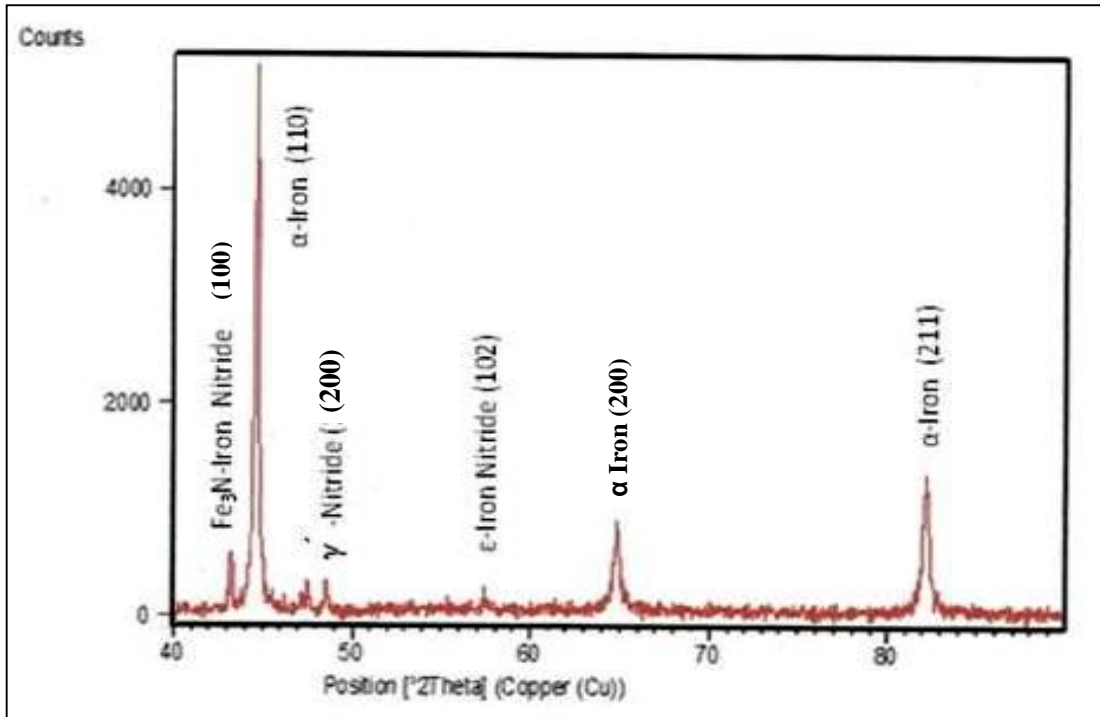


Fig. 4.54: X-ray diffraction (XRD) profile for plasma nitrided sample with compound layer thickness more than 10 microns shows peaks of α -iron , γ '-iron as well as ϵ -iron.

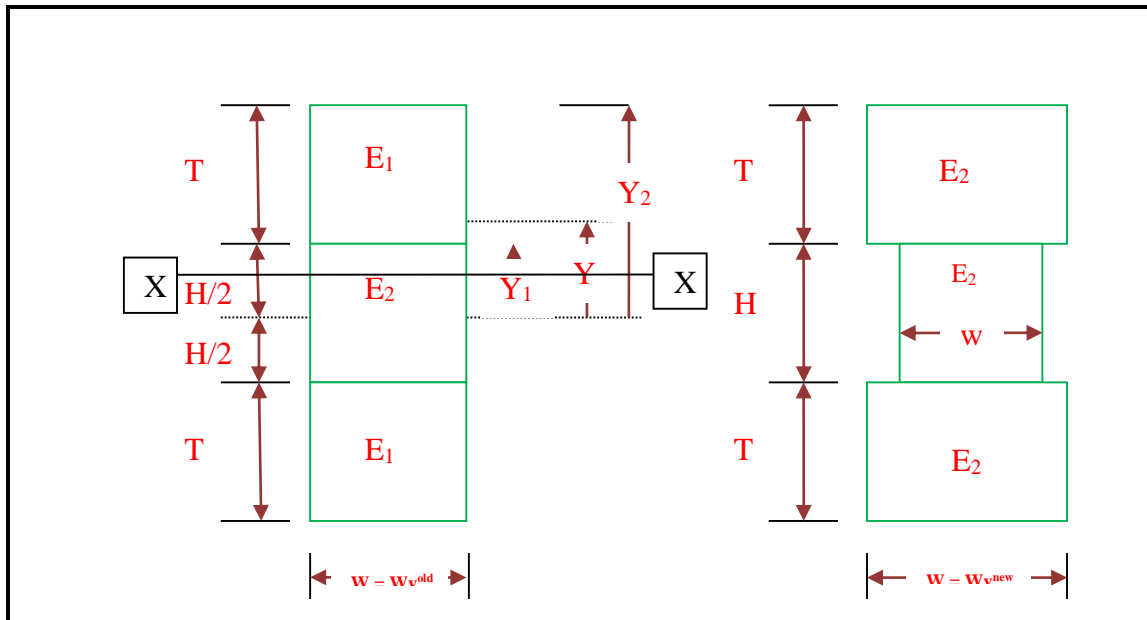
Peak search results:

Sr. No.	2-Theta	Relative intensity I / I ₀	Observed 'd' value	'd' value for standard sample	Plane (hkl)	Phase	JCPDS File No.
1	43.319	10.68	2.08702	2.09	100	Fe ₃ N - Iron Nitride	1-1236
2	44.713	100.00	2.02512	2.0268	110	α -Iron	6-06 96
3	47.63	5.04	1.90780	1.897	200	γ Iron Nitride	6-06 27
4	57.59	1..86	1.59927	1.59	102	ϵ -Iron Nitride	3-09 25
5	64.926	15.94	1.43510	1.4332	200	α -Iron	6-06 96
6	82.264	26.01	1.1703	1.1702	211	α -Iron	6-06 96

4.6 Finite Element Analysis to Determine Stress State in White Layer

4.6.1 Validation of FEM analysis procedure using closed form equivalent composite beam

For the purpose of validating the FEM analysis procedure, a composite beam as shown in Fig. 4.55 with neutral axis X-X was considered.



a) Original “actual” cross section

b) Transformed cross section

Fig.4.55: Composite beam considered for validation purpose

Nomenclatures used -

- Subscript “1” corresponds to white layer
- Subscript “2” corresponds to base material
- “W” is width and “T” is the thickness of the composite beam
- E1, E2 and E are elastic constant for white layer, base material and composite, respectively
- X-X is Neutral axis

With reference to Fig. 4.55, to enable the application of elementary “monolithic” beam theory, we need to convert the composite “E₁-E₂” cross-section into a monolithic E₂ (based material) cross-section. It can be shown that this can be accomplished by the following algorithm:

i] For every $y_1 \leq y \leq y_2$,

Change beam width W_y^{old} to new beam width W_y^{new} by transformation:

$$W_y^{\text{new}} = (E_1/E_2)(W_y^{\text{old}})$$

ii] The neutral axis of this equivalent beam will now coincide with its centroidal axis.

Thus, we can compute section stress, $\sigma_{zz}^{\text{Equiv}}$ by the flexural expression:

$$\sigma_{zz}^{\text{Equiv}} = -M_{xx}y/I_{xx}^{\text{Equiv}}$$

Where,

M_{xx} = Bending moment

Y = Outer fibre distance from neutral axis

I_{xx} = Area moment

iii] Next we need to normalize the equivalent stress, $\sigma_{zz}^{\text{Equiv}}$ to actual stress in original composite beam by:

$$\begin{aligned}\sigma_{zz}^{\text{actual}} &= (E_2^{\text{actual}}/E_1^{\text{transformed}})(\sigma_{zz}^{\text{Equiv}}) \\ &= (E_1/E_2)(\sigma_{zz}^{\text{Equiv}})\end{aligned}$$

In the present work, the above formulation has been used to compute the state of stress distribution in a rectangular cross-section beam by approximating the beam height to be equal to the diameter of the specimen.

Using the above formulation, along with assumptions, the peak state of stress, for a beam of rectangular cross-section of width “W” and height “H” is given as

$$\sigma_{zz}^{\text{Base}} = \frac{-M_{xx} \left(\frac{H}{2}\right)}{\frac{WH^3}{12}}$$

Similarly, for a composite beam of width “W” and thickness “T” along with elastic constant E_1 for white layer (elastic constant of base material being taken as E_2), the peak state of stress, $\sigma_{zz}^{\text{comp}}$ in the outer fiber would be :

$$\sigma_{zz}^{Comp} = \frac{-M_{xx} \left(\frac{H+2T}{2} \right)}{\left(\frac{WH^3}{12} + \left[2\alpha \frac{WT^3}{12} + \alpha WT \left(\frac{H+T}{2} \right)^2 \right] \right)}$$

Taking ratio of the above two equations, enables us to write:

$$\begin{aligned} \frac{\sigma_{zz}^{Comp}}{\sigma_{zz}^{Base}} &= \frac{(H+2T)}{H} \cdot \frac{\frac{WH^3}{12}}{\frac{W}{12} \left(H^3 + 2\alpha T^3 + 24\alpha T \left(\frac{H+T}{2} \right)^2 \right)} \\ &= \frac{(H+2T)H^2}{H^3 + 2\alpha T^3 + 6\alpha T(H+T)^2} \end{aligned}$$

where, $\alpha = \frac{E_1}{E_2}$

Finally, the actual sectional peak stress ratio, $\left(\frac{\sigma_{zz}^{Comp}}{\sigma_{zz}^{Base}} \right)_{actual}$ becomes -

$$\left(\frac{\sigma_{zz}^{Comp}}{\sigma_{zz}^{Base}} \right)_{actual} = \frac{\alpha(H+2T)H^2}{H^3 + 2\alpha T^3 + 6\alpha T(H+T)^2}$$

Taking $E_1 = 72$ GPa (say) and $E_2 = 207$ GPa (Standard value for steel), we have:

$$\frac{E_1}{E_2} = 0.35$$

With the above value of α , the ratio $\left(\frac{\sigma_{zz}^{Comp}}{\sigma_{zz}^{Base}} \right)_{actual}$ were computed as a function of different values of T.

4.6.2 Results of validation

The analysis of composite beam was carried out as mentioned above and also using FEM software “ANSYS -Version 15.0”. Data used for both these analyses is given in Table 4.12. These comparisons are presented in Table 4.13. Close fit was found between the FEA and closed forms solutions. Hence, it can be said that the FEA procedure used is validated.

Table 4.12: Data used for composite beam analysis

Parameters	Values
Thickness of base material, (mm)	25
Width of base material, (mm)	10
E_1 for coating, (GPa)	72
E_2 for Base material, (GPa)	207
I_{XX} (base material), (mm^4)	13020.83
σ_{XX} (monolithic), (N/mm^2)	4.80
Moment, (Nm)	5

Table 4.13: Results of composite beam analysis

Thickness of coating (mm)	Width of coating (new) (mm)	I_{XX} (mm^4)	σ_{XX} (transformed) N/mm^2	Calculated σ_{XX} (composite) (N/mm^2)	σ_{XX} (composite) (max) (N/mm^2) obtained through FEA
5.000	3.478	20919	3.59	1.454	1.45
2.000	3.478	15561	4.34	1.623	1.62
1.000	3.478	14197	4.58	1.653	1.67
0.500	3.478	13586	4.69	1.664	1.68
0.250	3.478	13298	4.75	1.667	1.69
0.100	3.478	13130	4.78	1.668	1.73
0.050	3.478	13075	4.79	1.669	1.71
0.025	3.478	13048	4.79	1.669	1.70

4.6.3 FEM analysis on actual fatigue geometry

A sub section of the fatigue specimens was modeled in SOLID WORKS 3D modeling package. This model was subsequently imported in to ANSYS version 15 FEM software and subjected to linear elastic-isotropic-stress analysis.

Typical output plots of this analysis are presented in Figs. 4.56 to 4.59. The results of elastic analysis are summarized in Tables 4.14 to 4.15 and are also summarized in Fig. 4.60 to 4.61.

In Fig. 4.60, plots for maximum normal fiber stress in Fe_4N and Fe_3N are compared as a function of white layer thickness varying from 5 μm to 20 μm . It can be noted from these plots that the peak stress in the Fe_{2-3}N phase is nearly 50% higher than in the Fe_4N phase. Further, it is also pertinent to note that significant variations in the value of the

peak stress as a function of white layer thickness do not exist for both phases. This lack of significant variation is essentially associated with the low thickness of the white layer.

In Fig. 4.61, plot of the state of maximum normal fiber stress is presented in the actual plasma nitrided fatigue specimen as a function of the thickness in the white layer from the surface of the base material. When we compare this plot with the peak normal stress in the base material, it is found that up to a distance of 10 μm in white layer the peak normal fiber stress is about 25% lower than the peak normal fiber stress in the base material. However, beyond a distance of 10 μm , the stress in the white layer rapidly switches over to a value which is nearly 30% higher than the peak normal fiber stress in the base material. The zone of “switching over” of the normal stress is due to presence of a two phase white layer zone of $\text{Fe}_4\text{N} + \text{Fe}_{2-3}\text{N}$.

Further, it has been found that the post- plasma nitriding residual stress in the white layer of Fe_{2-3}N constitution is of tensile orientation while that in the Fe_4N phase is of compressive orientation [2.92, 2.142, 2.148-150]. Thus, presence of tensile normal stress in the Fe_{2-3}N layer, (in white layer with thickness greater than 10 μm) will add to the externally applied bending stress creating further stress intensification resulting in further degradation of fatigue life.

In contrast, the compressive state of normal stress in Fe_4N white layer of thickness less than 10 μm , will subtract from the externally applied bending stress resulting in reduction in stress intensification and increase in fatigue life.

To summarize, the findings of the FEM stress analysis carried out in the present study confirm and support the fatigue life versus white layer thickness correlation found in the experimental program carried out in this work.

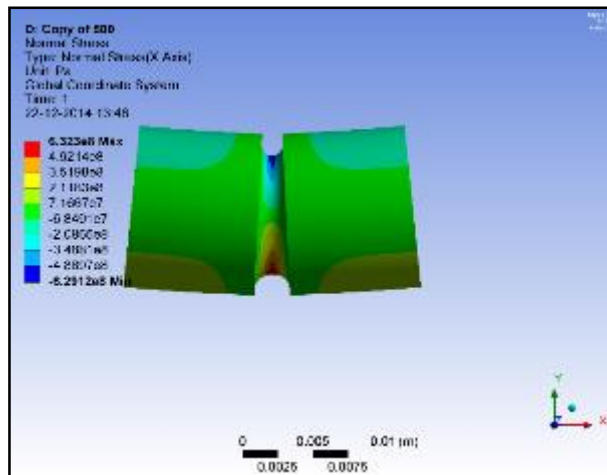


Fig. 4.56: Normal fiber stress in the untreated specimen

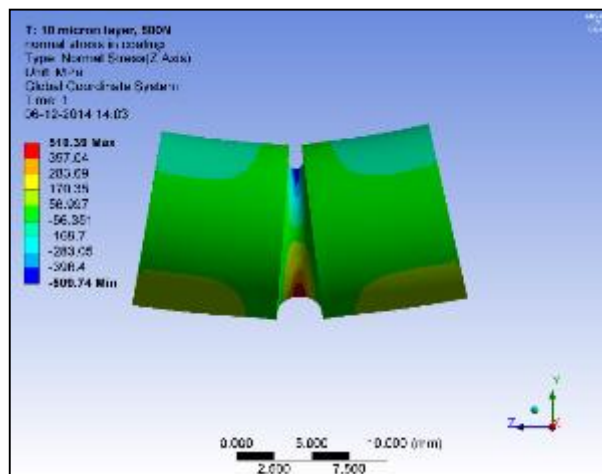


Fig. 4.57: Normal fiber stress in the Fe₄N white layer of thicknesses, T= 10 μm

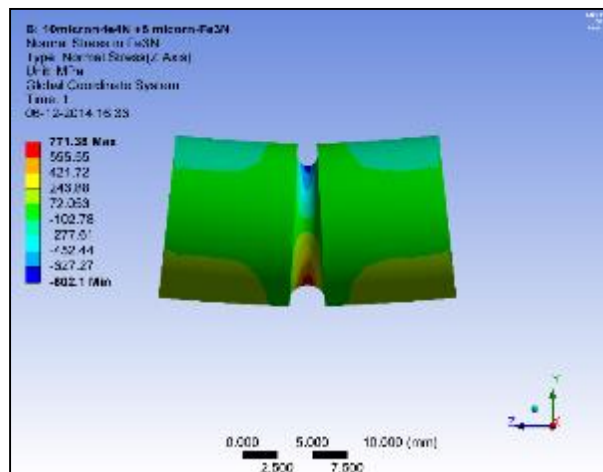


Fig. 4.58 Normal Fiber Stress in the Fe₂₋₃ layer of composite white layer of thicknesses of T (Fe₄N) = 10 μm + T (Fe₂₋₃N) = 5 μm

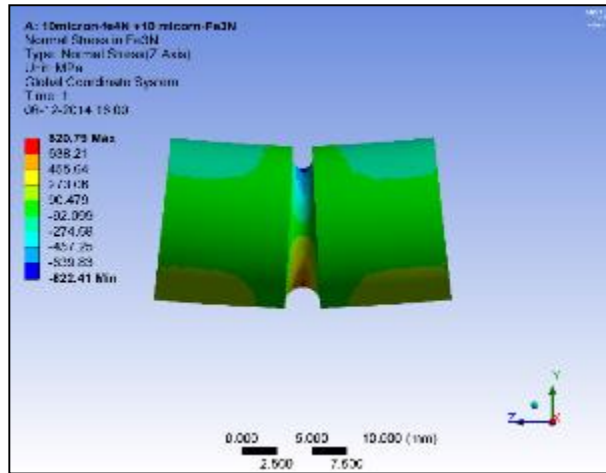


Fig. 4.59 Normal fiber stress in the Fe₂₋₃N layer in composite layer of thicknesses of T (Fe₄N) = 10 μm + T (Fe₃N) = 10 μm

Table 4.14: Max. normal stresses developed in single layer of Fe₄N

Thickness of layer, microns	Max. normal stresses, MPa
0 (Untreated)	639.30
5	515.56
10	510.39
20	534.59

Table 4.15: Max. normal stresses developed in single layer of Fe₂₋₃N layer

Thickness of layer, microns	Max. normal stresses, MPa
0 (Untreated)	639.30
5	727.64
10	728.03
20	746.32

Table 4.16: Max normal stresses developed in single layer of Fe₄N and composite white layer of Fe₄N + Fe₂₋₃N

Thickness of white layer, microns	Phases in white layer	Max normal stresses in Fe ₄ N (MPa)	Max normal stresses in Fe ₂₋₃ N (MPa)
0 (Untreated)	Fe ₄ N	639.3	--
5	Fe ₄ N	515.56	--
10	Fe ₄ N	510.39	--
15	Fe ₄ N (10 microns) + Fe ₂₋₃ N (5 microns)	--	771.38
20	Fe ₄ N (10 microns) + Fe ₂₋₃ N (10 microns)	--	820.79

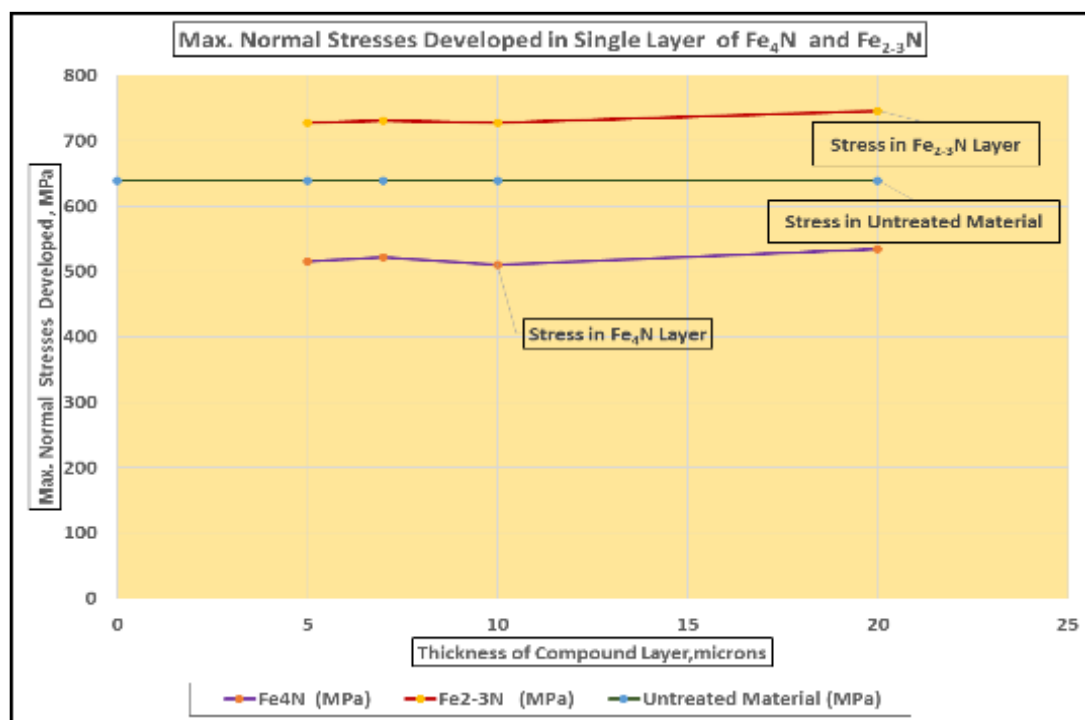


Fig. 4.60: Maximum Normal Fiber Stress in the untreated specimen and single layers of Fe₄N and Fe₂₋₃N shows that the peak stress in the Fe₂₋₃N phase is nearly 50% higher than in the Fe₄N phase

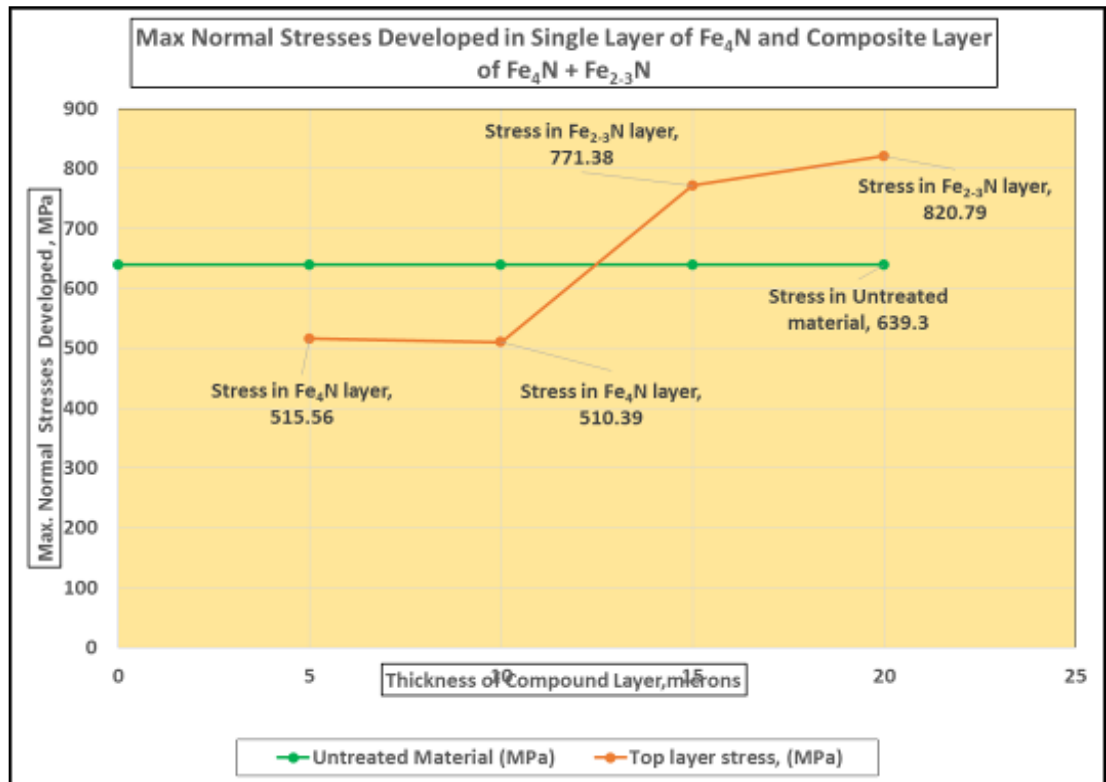


Fig. 4.61: Maximum Normal Fiber Stress in the untreated specimen, Fe₄N layer & Fe_{2.3}N layer of composite layer shows that up to a distance of 10 μm in white layer the peak normal fiber stress is about 25% lower while beyond a distance of 10 μm, the stress is nearly 30% higher than the peak normal fiber stress in the base material.

From the study it is observed that the fatigue life of steel is either reduced or increased due to surface treatments. Fatigue life is decreased by chromium plating, thermal spray coating and plasma nitriding process provided the compound layer thickness is not controlled, while it is increased with plasma nitriding without compound or with controlled thickness. The effect on fatigue life as well as strength is indicated by S-N curves, stress modification factor and cycle modification factors derived from fatigue data.

The S-N curves for surface treatments are compared with that of untreated (base) material. As the fatigue strength increases the S-N curve shifts upward. The fatigue strength modification factor is a ratio of stress required for given fatigue life cycle of a treated specimen to the stress required for untreated specimen for similar life cycle. Hence, when stress modification factor is equal to one the fatigue strength is unaffected, while if the ratio is more than one the fatigue strength increases, and if it less than one fatigue life decreases. The cycle modification factor is a ratio of fatigue life cycles for

a applied stress value on the treated specimen to the life cycles of untreated specimen for same value of applied stress. Hence, when cycle modification factor is equal to one the fatigue life for a given stress value is unaffected, while if the ratio is more than one the number of fatigue life cycles increases, and if it less than one number of fatigue life cycles decreases.

Chrome plating has adverse effect on fatigue life of steel. This is due to the residual tensile stresses developed in the plating and the strong coating / substrate interface adhesion. The presence of cracks in plating (observed in microstructural examination) are indication for residual tensile stresses in plating. Such residual tensile stresses develop stress concentration sites on the periphery of the specimen surface, and which become potential fatigue crack initiation sites. Ratchet marks observed on fracture surface of the fatigue tested specimen indicate presence of such multiple fatigue crack origins on the surface (Refer Fig. 4.40)

Similar to the chrome plated specimens, thermal spray coated specimens also affect fatigue life adversely. This is due to the residual tensile stresses developed due to coating on metal surface. Such residual tensile stresses develop stress concentration sites on the periphery of the specimen surface, and which become potential fatigue crack initiation sites. Ratchet marks observed on fracture surface of the fatigue tested specimen indicate presence of such multiple fatigue crack origins on the surface (Refer Fig. 4.42) The fatigue crack initiation has started from the interface between the coating and specimen surface.

Plasma nitriding treatment is seen to have beneficial effect on fatigue life provided compound layer thickness is controlled.

For the condition when no compound layer is formed plasma nitriding treatment as such improves the fatigue life due to increased hardness / strength of matrix at the diffusion layer (due to formation of nitrides) and high compressive residual stresses developed on surface. This has been indicated by the results on plasma nitrided specimens without compound layer. Improvement of fatigue strength to the extent of 150% of the untreated specimens is observed. Fracture surface of fatigue tested specimens indicate that there

is no stress concentration on the surface and hence, the fatigue crack initiation has taken place uniformly all over the surface similar to the untreated specimens.

For condition when compound layer is formed presence of compound layer has adverse effect on fatigue life. Hence, as the compound layer thickness increases the fatigue life is reduced. Fracture surface of specimens with compound layer more than 10 micron, shows ratchet marks indicating multiple crack origins due to higher stress concentration sites at surface.

Various phases present in compound layer i.e. Fe_4N & Fe_{2-3}N which have different mechanical properties. Considering the specimen as a composite beam consisting of base material with surface layers of Fe_4N and Fe_{2-3}N , it leads to generation of varying stresses in the surface layer. This has been observed through FEM analysis. For a given applied load, compound layer containing only Fe_4N phase reduces stress level in the surface as compared to untreated specimen, while the Fe_{2-3}N increases the stresses in the surface. During formation of compound layer, initially the relative amount of Fe_4N is more as compare to Fe_{2-3}N , while after a certain threshold value (in this case it is observed as 10 microns) the amount of Fe_{2-3}N is more than Fe_4N . This relates to FEM results which show that stresses generated in surface layer for below 10 micron thickness of compound layer are less than untreated condition. After 10 micron thickness value, the stresses are higher than untreated condition. This justifies the decrease in fatigue life for specimens with compound layer thickness value of more than 10 microns.

FEM study also indicate that maximum normal fiber stress in the Fe_{2-3}N phase is nearly 50% higher than in the Fe_4N phase. Furthermore, beyond a distance of 10 μm , the stress in the white layer rapidly switches over to a value which is nearly 30% higher than the peak normal fiber stress in the base material.

As soon as the thickness is higher than the threshold value the fatigue life starts decreasing. In the present study, the threshold is computed as 10 microns. Hence, below 10 micron thickness of compound layer, the fatigue life is higher than the untreated while fatigue life is less for more than 10 micron.